Reversible PCET and Ambient Catalytic

Oxidative Alcohol Dehydrogenation by {V=O}

Perfluoropinacolate Complexes

Jessica K. Elinburg, a Samantha L. Carter, Joshua J. M. Nelson, Douglas G. Fraser, Michael P.

Crockett, Aaron B. Beeler, Ebbe Nordlander, Arnold L. Rheingold, and Linda H. Doerrer

^a Department of Chemistry, Boston University, 590 Commonwealth Avenue, Boston, MA 02215,

USA. Email: doerrer@bu.edu.

^b Department of Chemistry, Boston College, 2609 Beacon Street, Chestnut Hill, MA 02467, USA.

^c Chemical Physics, Department of Chemistry, Lund University, Box 124, SE-221 00, Lund,

Sweden.

^d Department of Chemistry and Biochemistry, University of California, San Diego, 9500 Gilman

Drive, MC 0332, La Jolla, CA 92093, USA.

*indicates corresponding author

Keywords: alcohol oxidation, vanadium, vanadyl, fluorinated ligands

Abstract

A new air-stable catalyst for the oxidative dehydrogenation of benzylic alcohols under

ambient conditions has been developed. The synthesis and characterization of this compound and

1

the related monomeric and dimeric V(IV)- and V(V)-pin^F (pin^F = perfluoropinacolate) complexes are reported herein. Monomeric V(IV) complex (Me₄N)₂[V(O)(pin^F)₂] (1) and dimeric (μ-O)₂bridged V(V) complex $(Me_4N)_2[V_2(O)_2(\mu-O)_2(pin^F)_2]$ (3a) are prepared in water under ambient conditions. Monomeric V(V) complex (Me₄N)[V(O)(pin^F)₂] (2) may be generated via chemical oxidation of 1 under an inert atmosphere, but dimerizes to 3a upon exposure to air. Complexes 1 and 2 display a perfectly reversible V^{IV/V} couple at 20 mV (vs. Ag/AgNO₃) while a quasi-reversible V^{IV/V} couple at -865 mV is found for 3a. Stoichiometric reactions of 3a with both fluorenol and TEMPOH result in the formation of $(Me_4N)_2[V_2(O)_2(\mu-OH)_2(pin^F)_2]$ (4a), which contains two V(IV) centers that display antiferromagnetic coupling. In order to structurally characterize the dinuclear anion of 4a, {K(18C6)}⁺ counter-cations were employed, which formed stabilizing K... O interactions between the counter ion and each terminal oxo moiety and H-bonding between the oxygen atoms of the crown ether and µ-OH bridges of the dimer, resulting in $\{K(18C6)\}_2[V_2(O)_2(\mu-OH)_2(pin^F)_2]$ (4b). The formal storage of H₂ in 4a is reversible and protoncoupled electron transfer (PCET) from crystals of 4a regenerates 3a upon exposure to air over the course of several days. Furthermore, the reaction of 3a (2%) under ambient conditions with excess fluorenol, cinnamyl alcohol, or benzyl alcohol resulted in the selective formation of fluorenone (82% conversion), cinnamaldehyde (40%), or benzaldehyde (7%), respectively, reproducing oxidative alcohol dehydrogenation (OAD) chemistry known for VO_x surfaces and demonstrating, in air, the thermodynamically challenging selective oxidation of alcohols to aldehydes/ketones.

Introduction

The production of aldehydes and ketones from primary and secondary alcohols is a critical reaction in organic chemistry due to the ubiquity of these moieties in pharmaceuticals, consumer

products, polymer precursors, and as synthetic feedstocks for industrial processes.¹ Many alcohol oxidation reactions have been developed (Table 1), and, to date, stoichiometric reactions using organic oxidants are common practice. For example, hypervalent iodine compounds, such as the Dess-Martin periodinane² and 2-iodoxybenzoic acid (IBX)³, are commonly used in the laboratory, but their cost and potential explosiveness have limited their use on the industrial scale.⁴ Dimethylsulfoxide (DMSO) activated by various electrophiles is employed in the well-known Swern,⁵⁻⁷ Pfitzner-Moffat,⁸ Corey-Kim,^{9, 10} and Parikh-Doering¹¹ oxidations, however these reactions may include expensive reagents, stringent reaction conditions, or undesirable byproducts. Transition metal-containing compounds have also been used, especially high-valent Cr compounds such as the Collins reagent (CrO₃•2pyr),¹² pyridinium chlorochromate (PCC),^{13, 14} pyridinium dichromate (PDC),¹⁵ and CrO₃/H₂SO₄ (Jones oxidation)¹⁶, but the acute toxicity of Cr poses significant health and environmental risks.

The development of catalytic transition metal complexes capable of utilizing O₂ as a terminal oxidant is attractive due to the formation of environmentally benign byproducts such as H₂O or H₂O₂. A variety of catalytic aerobic alcohol oxidation reactions utilizing transition metal complexes has been established, most notably with Pd(II)^{17, 18} and Cu(I)/TEMPO,¹⁹⁻²¹ although these systems can be subject to catalyst decomposition over time or are constrained by the use of stoichiometric additives.

Table 1. Overview of common alcohol oxidation systems and comparison to soluble V systems.

System	Stoichiometric/ catalytic	Conditions required	Substrate scope	Other considerations
--------	------------------------------	------------------------	-----------------	----------------------

Dess-Martin ² periodinane	Stoichiometric	Air, RT		Expensive, potentially explosive, poor stability
Swern ⁵⁻⁷ activated DMSO	Stoichiometric	Air, -78°C to -30°C		Formation of Me ₂ S and CO
Jones ¹⁶ Cr	Stoichiometric	Air, 0°		Highly exothermic; poor selectivity; toxicity of Cr
Stahl ¹⁹⁻²¹ Cu(I)/TEMPO	Catalytic	Air, RT	Benzylic, allylic, aliphatic alcohols	TEMPO/ABNO required
{(V(O) ₄)(Hpic) ₄ } ²² (Hpic = 3-hydroxypicolinate)	Catalytic	1.0 MPa O ₂ , 120°C	Benzylic alcohols	Autoclave needed for high O ₂ pressure
{(V(O)4)(Hpic)4} ²² (Hpic = 3-hydroxypicolinate) [V(O)(HQ) ₂ O ⁱ Pr] ²³ (HQ = 8-hydroxyquinolinate)	Catalytic Catalytic			needed for high
(Hpic = 3-hydroxypicolinate) [V(O)(HQ) ₂ O ⁱ Pr] ²³		120°C Air, 40°C to	alcohols Benzylic	needed for high O ₂ pressure Base (Et ₃ N) assisted; not

In the realm of heterogeneous catalysis, surface-supported vanadium oxides (VO_x) are among the most efficient catalysts for the aerobic oxidative dehydrogenation of both alkanes and alcohols.²⁵⁻³⁹ In these systems, vanadium is deposited onto an oxide support, most commonly MgO, Al₂O₃, ZrO₂, TiO₂, or SiO₂, forming monomeric or polymeric VO_x moieties on the surface (Figure 1). The speciation and product distribution of oxidative alcohol dehydrogenation (OAD) reactions effected by supported VO_x catalysts is largely dependent on the pH of the specific support utilized and selectivity can be difficult to control, resulting in mixtures of aldehydes/ketones, carboxylic acids, ethers, and CO_x.^{37, 38} Furthermore, the limited spectroscopic characterization available to heterogeneous systems often prevents obtaining detailed mechanistic information.

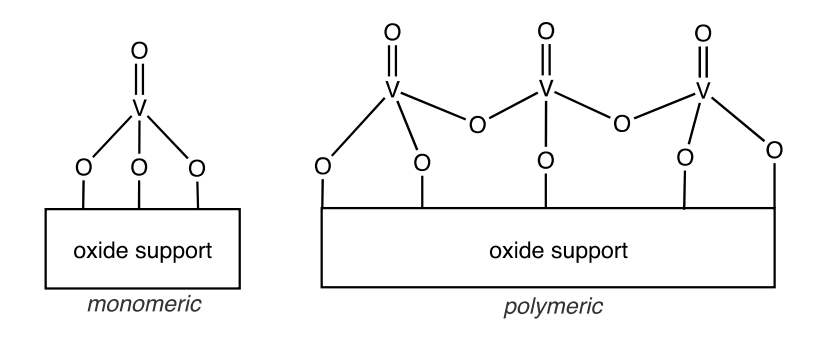


Figure 1. Surface-supported monomeric and polymeric VO_X units.

Figure adapted from Wachs et al., ref #37

Soluble oxidovanadium complexes have also been utilized as catalysts for aerobic OAD.^{22, 23, 40} Research to date has largely focused on reactivity of terminal oxo moieties in monomeric systems, although work by Mayer *et al.* concludes that H-atom transfer (HAT) to terminal oxo moieties in V=O complexes proceeds slowly due to a high intrinsic reorganization barrier resulting from structural changes in the molecule upon HAT.⁴¹ On the other hand, deriving inspiration from heterogeneous systems, the extended (μ-O)-bridged structures utilized in VO_x surface chemistry are a promising motif for HAT. In bridging systems, the Lewis-basic μ-O sites can serve as proton

acceptors and the redox-active V center can accept reducing equivalents while circumventing the energetic barrier associated with HAT to a terminal V=O moiety that rearranges.

Limberg and coworkers have explored this concept with $(\mu\text{-O})$ -bridged V dimers featuring incompletely condensed silsesquioxane, ⁴²⁻⁴⁴ calixarene, ⁴⁵⁻⁴⁷ thiacalixarene, ²⁴ and thiobisphenol ^{48, 49} ligands. Not only do these systems catalyze OAD, but mechanistic investigations have been carried out that corroborate Mayer's findings concerning the relative HAT reactivities of terminal versus bridging oxo moieties. Studies of the V=O thiacalixarene system revealed that upon dissolution, the $(\mu\text{-O})$ -bridged V(V) dimer enters into an equilibrium with a monomeric form, and experiments confirm that the dimeric complex is solely responsible for catalysis, indicating the μ -O bridge as necessary in HAT. ⁵⁰

Recent work by Doerrer and coworkers has focused on the formation of Earth-abundant transition metal complexes featuring oxidatively robust highly fluorinated alkoxide ligands. $^{51-62}$ As weak π -donors, these ligands are significantly less nucleophilic than their hydrogenated counterparts and can be air- and water-stable. In this work, we report a group of monomeric and dimeric V(IV) and V(V) complexes of perfluoropinacolate, $(pin^F)^{2-}$. The monomeric V(IV) complex $(Me_4N)_2[V(O)(pin^F)_2]$ (1) was prepared in water under ambient conditions. Recrystallizations of 1 left in air over long periods of time led to the unexpected formation of the dimeric complex $(Me_4N)_2[V_2(O)_2(\mu-O)_2(pin^F)_2]$ (3a) in low yield. The V(V) dimer 3a features two oxidized V centers bridged by two $(\mu-O)_2$ units, a scaffold primed for HAT and OAD, as demonstrated by Limberg's important precedent. Herein, the synthesis, spectroscopic characterization, and OAD reactivity of V-pin^F complexes under mild, ambient conditions are presented and stoichiometric proton-coupled electron transfer (PCET) reactions to 3a and catalytic OAD are demonstrated.

Results and Discussion

Synthesis of complexes 1, 2, 3a, and 4a.

$$V(O)SO_4 + 2 \xrightarrow{F_3C} \xrightarrow{OH} \xrightarrow{CF_3} + 4 \text{ Me}_4 \text{NOHSH}_2O$$

$$V(O)SO_4 + F_3C \xrightarrow{OC} \xrightarrow{OC} \xrightarrow{CF_3} + 2 \text{ Me}_4 \text{NOHSH}_2O$$

$$V(O)SO_4 + F_3C \xrightarrow{OC} \xrightarrow{OC} \xrightarrow{CF_3} + 2 \text{ Me}_4 \text{NOHSH}_2O$$

$$V(O)SO_4 + F_3C \xrightarrow{OC} \xrightarrow{OC} \xrightarrow{CF_3} + 2 \text{ Me}_4 \text{NOHSH}_2O$$

$$V(O)SO_4 + F_3C \xrightarrow{OC} \xrightarrow{OC} \xrightarrow{OC} \xrightarrow{OC} \xrightarrow{OC} \xrightarrow{CF_3} \xrightarrow{F_3C} \xrightarrow{OC} \xrightarrow{OC} \xrightarrow{OC} \xrightarrow{CF_3} \xrightarrow{F_3C} \xrightarrow{OC} \xrightarrow{OC} \xrightarrow{OC} \xrightarrow{CF_3} \xrightarrow{F_3C} \xrightarrow{OC} \xrightarrow$$

Scheme 1. Syntheses of V-pin^F complexes 1, 2, 3a, and 4a.

The synthesis of 1 was carried out in a mixture of $H_2O/MeOH$ under ambient conditions, similar to the procedure originally carried out by Willis.⁶³ In crystalline form, 1 is markedly air- and water-stable. Interestingly, when solutions of 1 were left open to air over the course of several weeks, the formation of several bright yellow crystalline blocks amongst the blue needles of 1 was observed. Single-crystal X-ray diffraction analysis revealed this yellow species to be the bis- μ -O-bridged V(V) dimer, 3a. The transformation of $(Me_4N)_2[V(O)(pin^F)_2]$ (1) to $(Me_4N)_2[V_2(O)_2(\mu$ -

O)₂(pin^F)₂] (**3a**) is not quantitative with respect to the ligand, requiring the formal loss of one equivalent of (pin^F)²⁻ ligand per V center. The direct, deliberate synthesis of **3a**, however, can be achieved using reaction conditions similar to those used for **1** and employing H₂O₂ in CH₃CN as an exogenous oxidant. This oxidation process was quite exothermic, likely due to the reaction of CH₃CN and H₂O₂ to form peroxyacetimidic acid (PAIA), a strong oxidant classically utilized in alkene epoxidation reactions.^{64, 65}

While 3a is air- and water-stable, attempts to synthesize 3a in other polar solvents such as acetone, THF, and 1,2-dimethoxyethane (DME) were unsuccessful, resulting in low yields of pale yellow oils. Furthermore, dissolving crystalline 3a in these solvents caused apparent transformation of the bright yellow complex into pale yellow oily solids with reduced solubility. While attempts to isolate and characterize the unexpected product(s) were unsuccessful, we hypothesize that polar, O-donor solvents may coordinate to the oxophilic V centers, effecting the cleavage of the bis-μ-O bridge to form two monomeric V(V) centers with two terminal oxo moieties (Scheme 2).

Marzilli and coworkers observed a similar phenomenon when N-donor ligands were introduced to the non-fluorinated osmium pinacolate complex, [Os₂(O)₂(μ-O)₂(pin)₂].⁶⁶ Addition of monodentate N-donor ligands such as pyridine induced the monomerization of their Os(VI) dimer resulting in the formation of octahedral monomeric complexes containing two terminal oxo groups and two equivalents of pyridine. While **3a** is stable in the presence of CH₃CN and triethylamine, O-donor solvents seem to effect a similar transformation in our system. ¹⁹F NMR spectroscopic studies of **3a** in several O-donor solvents corroborate this hypothesis (Figure S1). The ¹⁹F NMR spectrum of **3a** in d₃-acetonitrile reveals the expected dimer, whereas in d₆-DMSO, a monomeric species similar to the V(V) complex (Me₄N)[V(O)(pin^F)₂] (**2**) (*vide infra*) is present.

Interestingly, in d₆-acetone, the spectrum of **3a** displays both monomeric/dimeric character, suggesting an equilibrium between the two forms. Except in the case of very strong O-donor solvents (such as DMSO), this monomerization is reversible and redissolving the monomeric form of **3a** in CH₃CN reforms the original dimeric complex.

Scheme 2. Hypothesized reaction of 3a with polar, O-donor solvents (shown here with THF). Gold color indicates V(V).

The isolation and relative stabilities of 1 and 3a suggested that a monomeric V(V) perfluoropinacolate complex, 2, might be isolated in the absence of O₂. Indeed, under N₂, addition of Ag⁺ to 1 in CH₃CN and subsequent recrystallization yielded orange blocks of 2. While crystalline samples of 2 are air-stable for several hours, exposing solutions of 2 to O₂ results in the rapid formation of 3a in low yield, confirmed via X-ray crystallographic analysis. The other products of this reaction are not known. We have previously reported oxidative cleavage of the pin^F central C-C bond and ligand conversion,⁶⁰ but that reaction of a Co(III) complex was much cleaner. Reaction of 3a with H-atom donors such as fluorenol and TEMPOH resulted in the formation of 4a, a reduced V(IV) dimer bridged by two bis-μ-OH groups. Exposure of 4a to air results in the reformation 3a.

Structural characterization of monomeric V-pin^F complexes 1 and 2.

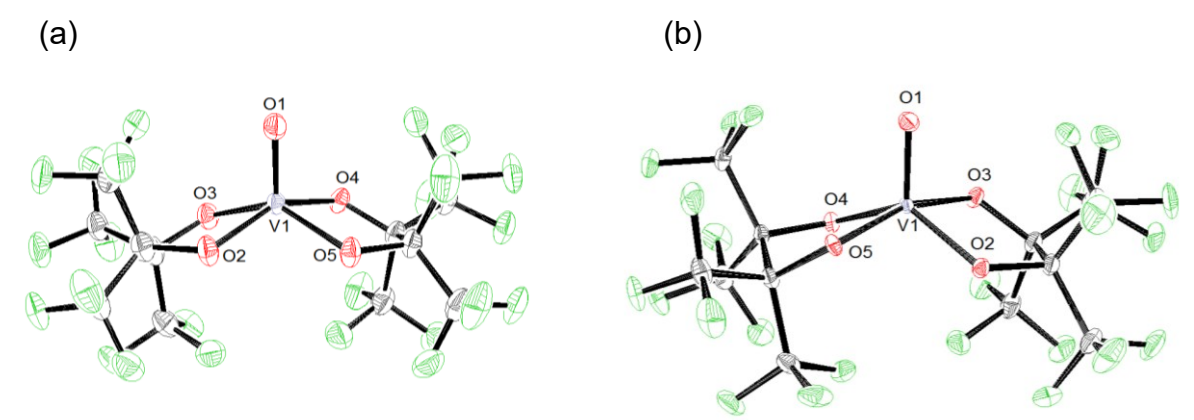


Figure 2. ORTEPs of the anions of (a) **1**, (Me₄N)₂[v(O)(pin⁻)₂] and (b) **2**, (Me₄N)[v(O)(pin⁻)₂]. Counter cations omitted for clarity. Ellipsoids are shown at the 50% probability level.

Important metrical parameters for **1** and **2** are summarized in Table 2; crystallographic data collection and refinement parameters are collated in Table S2. The molecular structure of the anion of **1** is shown in Figure 2a. The five-coordinate V(IV) center is coordinated by a single terminal oxo moiety and two bidentate $(pin^F)^{2-}$ ligands with a distorted square pyramidal geometry ($\tau_5 = 0.20$).⁶⁷ The bond length between V and the terminal oxygen is 1.61 Å and the average V—O distance between the V center and the $(pin^F)^{2-}$ ligand is 1.96(1) Å with the orientation of each $(pin^F)^{2-}$ ligand slightly skewed such that one side of each chelate ring is slightly longer. The O₄ basal plane lies slightly below the V center. The O(pin^F)—V=O bond angles in **1** range from 103 to 110° and within the ligand, adjacent O(pin^F)—V—O(pin^F) bond angles span 80 to 92° and transverse O(pin^F)—V—O(pin^F) bond angles span 141 to 153°, distorting the complex from approximate C_{4v} symmetry..

Complex 2 (Figure 2b) crystallizes with two crystallographically independent molecules in the asymmetric unit; crystallographic data for only one of the two anions are included in Table 2. Similar to 1, the five-coordinate V(V) center is coordinated to a single terminal oxo moiety and

two bidentate $(pin^F)^{2-}$ ligands and the geometry of the complex lies between square pyramidal and trigonal bipyramidal ($\tau_5 = 0.50$). The V=O bond length is 1.58 Å and the average V—O distance between the V center and alkoxide O atoms is 1.88(2) Å. Compared to 1, a decrease of only 0.03 Å in the V=O bond length of 2 is observed; the increased electrostatic interaction effected by the oxidized V center is more evident in the decreased V—O bond distances between the metal center and the $(pin^F)^{2-}$ ligand. In this complex, the displacement of V from the $\{O_4\}$ plane is more pronounced with $O(pin^F)$ —V=O bond angles ranging from 98 to 114°, compared to the smaller range observed in 1. Within the ligand, adjacent $O(pin^F)$ —V— $O(pin^F)$ bond angles of 2 span from 81 to 94°, a similar range to that of 1, while the range of transverse $O(pin^F)$ —V— $O(pin^F)$ bond angles is significantly larger than that of 1.

Although 1, 2, and 3a, were readily synthesized as Me₄N⁺ salts, initial attempts to structurally characterize 4a were unsuccessful due to significant disorder within the crystals. The crystal structure of the V(IV) (μ-OH)₂-bridged dimer 4b was ultimately obtained by employing {K(18C6)}⁺ as the counter-ion, using the {K(18C6)}⁺ salt 3b as starting material. Crystallographic data for 3b and 4b are summarized in Table 3; crystallographic data for 3a are included in the SI. Overall, the crystal structures of 3b and 4b (Figure 3) reveal that the {K(18C6)}⁺ counter-ion offers K⁻⁻O, K⁻⁻F, and hydrogen bonding interactions that are not present in the Me₄N⁺ analogs 1 and 2. While the introduction of stabilizing {K(18C6)}⁺ counter-cations ultimately allowed for the crystallographic characterization of 4b, Me₄N⁺ analog 4a crystallized in much higher yield, and as shown in the experimental characterization section, the two analogs are virtually spectroscopically identical, except for cation-based ¹H-NMR signals. Therefore, the (Me₄N)⁺ derivatives 3a and 4a were used in all reactivity studies.

Table 2: Selected bond lengths (Å) and angles (°) for 1 and 2.

O _a w _o U O _c		1	2
Selected bond lengths (Å			
V=O	-)	1.609(3)	1.582(2)
	V—O _a	1.955(2)	1.864(2)
	V—O _b	1.974(3)	1.899(2)
V—O (pin ^F)	V—O _c	1.969(2)	1.870(2)
	V—O _d	1.949(2)	1.878(2)
Selected bond angles (°)			
3 ()	O _a —V=O	109.95(13)	113.46(11)
	O _b —V=O	103.84(13)	98.01(10)
O(pin ^F)—V=O	O _c —V=O	103.30(12)	99.25(10)
	O _d —V=O	109.25(12)	113.95(11)
O(pin ^F)—V—O(pin ^F)	O _a —V—O _b	80.34(10)	81.00(9)
	O_b — V — O_d	91.66(10)	90.21(9)
	O_c — V — O_d	80.62(10)	81.08(9)
	O _a —V—O _c	89.25(10)	93.80(9)
	O_a — V — O_d	140.77(11)	132.53(9)
	O _b —V—O _c	152.83(11)	162.64(9)
τ_5^{67}		0.20	0.50

Structural characterization of dimeric V-pin F complexes 3b and 4b.

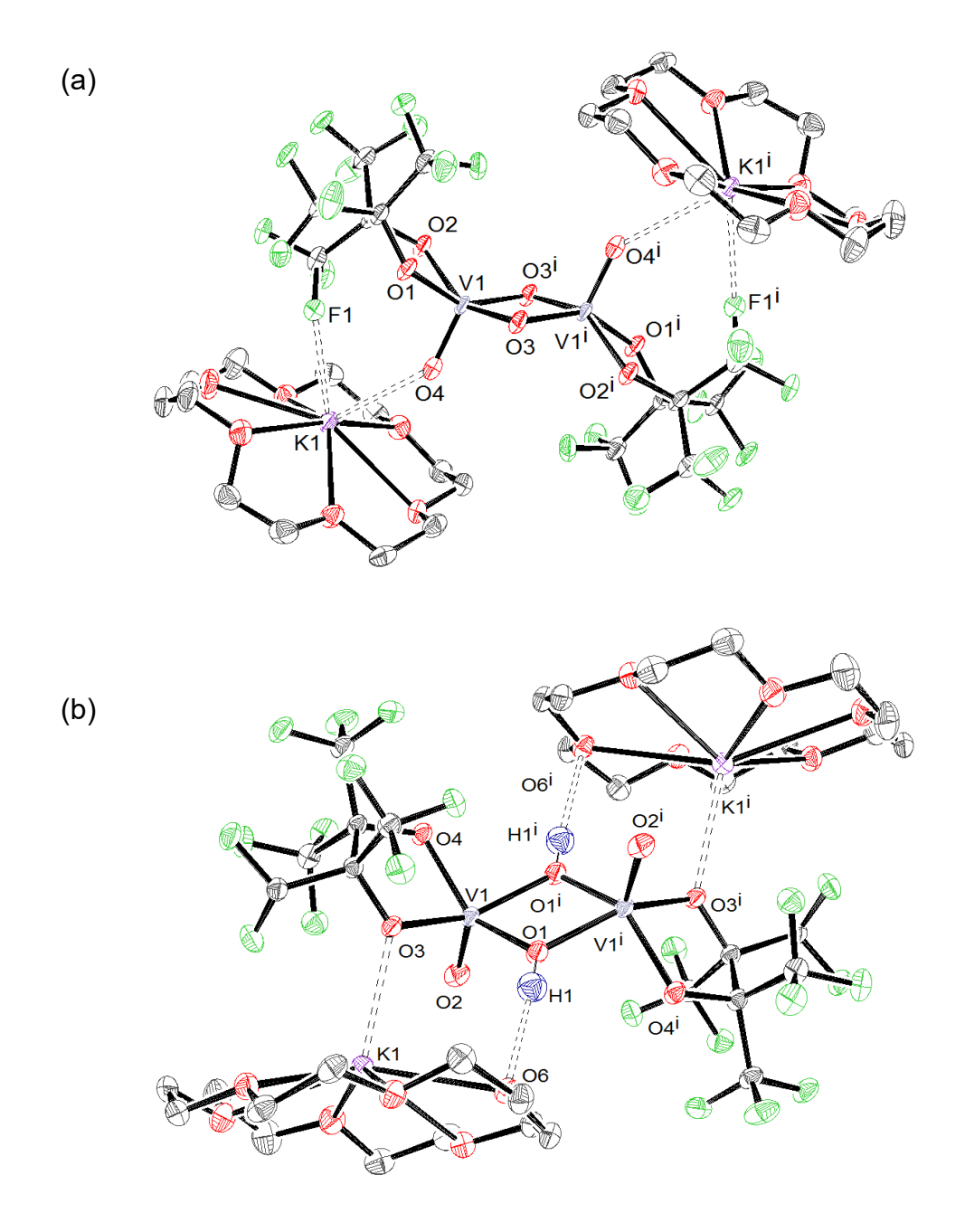


Figure 3. ORTEPs of (a) **3b**, $\{K(18C6)\}_2[V(O)_2(\mu-O)_2(pin^F)_2]$ and (b) **4b**, $\{K(18C6)\}_2[V(O)_2(\mu-O)_2(pin^F)_2]$. H atoms, except those in the $(\mu-OH)$ bridge, omitted for clarity. Ellipsoids shown at the 50% probability level.

Complex 3b (Figure 3a) comprises two crystallographically equivalent V(V) centers in a nearly perfect square pyramidal configuration ($\tau_5 = 0.02$), ⁶⁷ each with a single terminal oxo in relative trans disposition and a (pin^F)²⁻ ligand, bridged by two (μ-O) moieties. Two K⁺ countercations, each encapsulated by one equivalent of 18-crown-6, lie symmetrically distributed above and below the dimer, with K... O interactions (2.91 Å) between K⁺ and the terminal oxo moiety; furthermore, K... F interactions are also present between K⁺ and an F atom on the (pin^F)²⁻ ligand (2.85 Å). The average V—O distance between the V center and the (pin^F)²⁻ ligand is 1.94(1) Å while the average V—(μ-O) distance is significantly shorter (1.82(4) Å) than the analogous V— O (pin^F) bond distance in 2. The V₂O₂ bridge is nearly perfectly symmetrical with a V—O—V bond angle of 96° and O(μ-O)—V=O bond angles of 107 and 108°; the distance between the two V centers is 2.71 Å. The (pin^F)²⁻ ligands are tilted downward from the V₂O₂ plane with O(pin^F)— V=O angles of 106°. Between adjacent ligands, the two O(pin^F)—V—O(μ-O) bond angles are very similar (88 and 89°) while the angles between transverse ligands are similarly consistent (146 to 147°). The singular O(pin^F)—V—O(pin^F) internal angle is 80°.

Complex **4b** (Figure 3b) comprises two crystallographically identical reduced V(IV) centers, each binding a single terminal oxo and (pin^F)²⁻ ligand, bridged by two (μ-OH) moieties. Notably, K··· O interactions (2.74 Å) between the K⁺ counter-ions and terminal oxo moieties are present, but unlike **3b**, no close (< 3.0 Å) K··· F interactions are observed. On the other hand, a H-bonding interaction (2.10 Å) between the protons of the (μ-OH)₂ bridge and an O atom of the crown ether rings is present. Formal addition of H₂ to **3b** to form **4b** shifts the K(18C6)⁺ moieties, resulting in diminished K··· F interactions, but establishing closer K··· O contacts and H-bonding

interactions. As in the case of the other {V(IV)(O)pin^F}-containing 1, the V=O bond length (1.60 Å) remains unaffected by the change in oxidation state; the reduction of the V centers is most conspicuously corroborated by the elongation of the $\{V_2O_2\}$ rhomb. Compared to **3b**, the average V—(μ-O) bond length is increased by 0.15 Å and the distance between the two V centers is expanded by 0.4 Å. Additionally, a slight lengthening (0.02 Å) of the average V—O bond lengths between the V center and the (pin^F)²⁻ ligand is observed. The hydrogen bonds between each proton of the (µ2-OH) bridges and an O atom of the crown ether draws the V-(µ2-OH)-V bridges outward, manifested by a simultaneous 8° decrease in the (μ-O)—V—(μ-O) angle and 8° an increase in V— O—V (μ-O) angle. Unlike 3b, the coordination environment around the two V centers in 4b deviates from perfect square pyramidal geometry ($\tau_5 = 0.17$).⁶⁷ While the two (μ -OH)—V=O angles are similar (107 and 108°), distortion from C_{4v} symmetry arises from the tilting of the (pin^F)²⁻ ligand downwards with asymmetric O(pin^F)—V=O angles of 103 and 113°. The O(pin^F)— V—O(μ-O) angles between adjacent ligands are similar (90 and 92°) while the angles between transverse ligands span from 139 to 149°. The singular O(pin^F)—V—O(pin^F) angle (79°) is slightly smaller than that of the V(V) dimer.

Table 3: Selected bond lengths and angles for **3b** and **4b**.

O _a ()	o _c	3b	4b		
Selected bond lengths (Å)					
V=O		1.598(4)	1.5954(14)		
V O (ninF)	V—O _a	1.928(4)	1.9732(12)		
V—O (pin ^F)	V — O_b	1.947(4)	1.9458(12)		
V—O (μ-O)	V—O _c	1.790(3)	1.9651(13)		

	V—O _d	1.844(4)	1.9646(13)		
Selected angles (°)					
O(pin ^F)—V=O	O _a —V=O	105.73(18)	103.44(6)		
	O _b —V=O	105.98(18)	112.89(6)		
Ο(μ-Ο)—V=Ο	O _c —V=O	107.98(19)	107.65(6)		
	O _d —V=O	106.71(18)	107.18(7)		
O(pin ^F)—V—O(pin ^F)	O _a —V—O _b	79.12(15)	81.17(6)		
Ο(μ-Ο)—V—(μ-Ο)	O _c —V—O _d	83.59(16)	75.92(6)		
O(pin ^F)—V—O(μ-O)	O _a —V—Oc	89.82(15)	91.75(5)		
	O_b — V — O_d	88.67(16)	90.01(5)		
	O_a — V — O_d	147.37(17)	149.19(6)		
	O _b —V—O _c	145.96(17)	139.41(6)		
V—O—V (μ-O)		96.41(16)	104.08(6)		
τ ₅ ⁶⁷		0.02	0.17		

Magnetic susceptibility and ¹H-, ¹⁹F-NMR spectroscopy of 1, 2, 3a, and 4b.

Figure 4. Isomers of **3a**. Unique CF₃ groups shown in purple (proximal to oxo) and green (distal to oxo). Gold color indicates V(V).

The solution-state magnetic susceptibility (μ_{eff}) of 1 is 1.42(5) μ_{B} , slightly lower than the d^{l} spin-only value of 1.73 μ_{B} , suggesting some solution instability of the V(IV) monomer. The

solution-state magnetic susceptibility of V(IV) dimer **4b** is even lower, 1.14(1) μ_B , suggesting substantial antiferromagnetic (AFM) coupling between the two V(IV) centers. Variable-temperature SQUID data (Figure S2) are consistent with this behavior, showing some increased coupling with decreasing temperature.

While the ¹H NMR spectra of diamagnetic 2 and 3a display only a single peak corresponding to their Me₄N⁺ counter cations, their ¹⁹F NMR spectra are much richer (Figure S3). The ¹⁹F NMR spectrum of **3a** displays four peaks ranging from -70.5 ppm to -71.2 ppm. These four features correspond to the four unique CF₃ environments present in the two possible configurational isomers of **3a** (Figure 4). While in the solid state, X-ray crystal diffraction data of 3a show that the two oxo groups of the V(V) dimer lie anti to one another, the ¹⁹F NMR spectrum suggests that in solution, a mixture of syn (with $\sim C_{2\nu}$ symmetry) and anti (with $\sim C_{2h}$ symmetry) forms is present. For each isomer, two CF₃ resonances, proximal and distal to the terminal oxo groups, are observed. The observed four-line pattern in the 19 F NMR spectrum ($S = \frac{1}{2}$) of 3a is analogous to the ¹H NMR pattern ($S = \frac{1}{2}$) observed for the non-fluorinated osmium pinacolate dimer, $[Os_2(O)_2(\mu-O)_2(pin)_2]$, initially studied by Marzilli et al. This isomerism was later corroborated by Casey in response to claims that reaction intermediates were responsible for the "extra" peaks. 66, 68, 69 Additionally, the four 19F NMR resonances of 3a are split by long-range coupling to the 51 V center (S = 7/2), although only quartets are visible, rather than the expected eight-line pattern, due to the three-atom (four-bond) separation between the V and the F. The ¹⁹F NMR spectrum of 2 contains two peaks at -70.03 ppm and -71.07 ppm, corresponding to the two possible CF₃ configurations within the monomeric V-pin^F species. Similar to **3a**, the CF₃ peaks are further split into apparent triplets by long-range coupling to the NMR-active 51 V nucleus (S =7/2, 99% abundance).

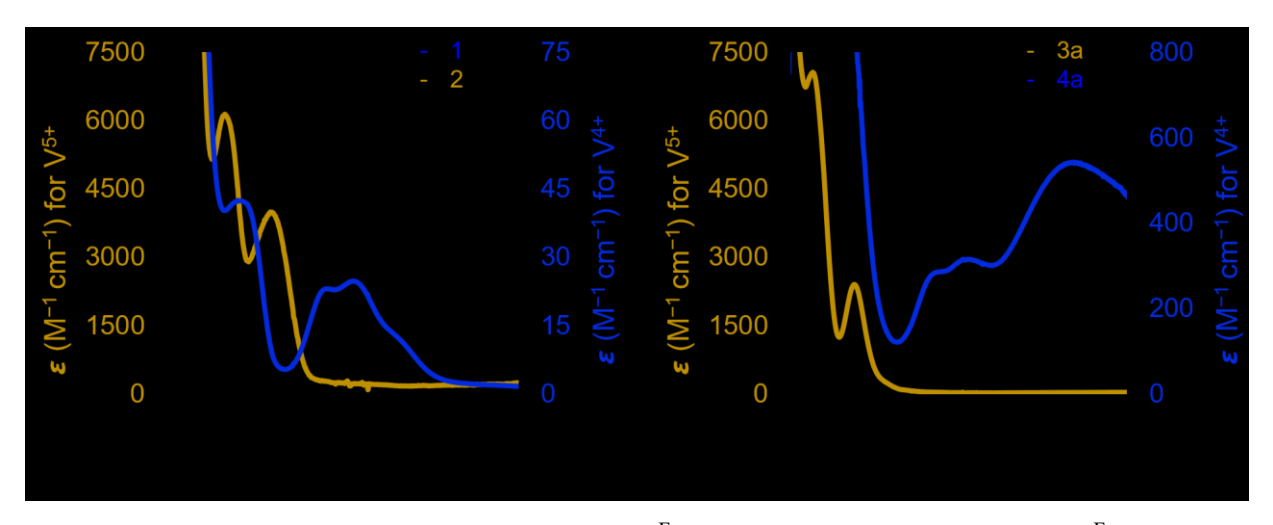


Figure 5. UV-visible absorption spectra of V-pin^F complexes in CH₃CN; (a) V-pin^F monomers **1** (blue) and **2** (gold); (b) V-pin^F dimers **3a** (gold) and **4a** (blue).

The UV-visible absorption spectra of 1, 2, 3a, and 4a are shown in Figure 5. The absorption spectra of mononuclear V(IV) vanadyl complexes with $\{V(=O)O_4\}$ cores have been well-understood for decades. In the visible range, V(IV) monomer 1 displays two d-d transitions at 564 and 624 nm, as well as a single higher-energy shoulder at 361 nm; similar to the spectrum observed by Willis. These features exhibit low extinction coefficients as expected for spin-forbidden electronic transitions within a single d1 center. In contrast, V(V) monomer 2 reveals two intense ligand-to-metal charge transfer (LMCT) bands at 330 and 438 nm; as anticipated, no d-d transitions are observed for the oxidized d0 center. The spectrum of V(V) dimer 3a is quite similar to that of 2, with two charge transfer bands at 252 and 355 nm, although the features are both blueshifted by about 80 nm.

The spectrum of $\mathbf{4a}$ reveals two d-d transitions at 543 and 625 nm, similar to those observed for $\mathbf{1}$, corroborating the reduction of both V(V) centers of $\mathbf{3a}$ upon PCET. Furthermore, a broad

feature at 870 nm is present in the spectrum of 4a, suggesting inter-valence charge transfer $(IVCT)^{71}$ between the two d^1 centers and the transient formation of a mixed-valent V(V)/V(III) dimer.

Cyclic voltammetry of 1, 2, 3a, and 4a.

The cyclic voltammograms of 1, 2, 3a, and 4a in CH₃CN under N₂ are shown in Figure 6. The voltammogram of 1 displays a single electrochemically reversible V^{IV/V} couple at 20 mV (vs. Ag/AgNO₃). The reversibility observed for this couple is corroborated by the straightforward isolation of 2 via Ag⁺ oxidation of 1 under inert atmosphere described above with a virtually identical V^{IV/V} redox couple at 20 mV. The voltammogram of 2 also includes an unexpected feature centered at -255 mV, corresponding to the oxidation of small amounts of residual Ag present in the sample. Although the presence of Ag was undetectable by elemental analysis, repeated recrystallizations of the sample proved unsuccessful in completely eliminating the impurity. Cyclic voltammetry measurements of 1 in air exhibited the same reversible V^{IV/V} redox couple at 20 mV at fast scan rates (over 250 mV/s) (Figure S5), but slowing the scan rate resulted in a clear loss of reversibility as the oxidation and subsequent dimerization of 1 to 3a to 2 is observable at sufficiently slow scan rates, corroborating synthetic observations. This process is predictably irreversible due to the formal loss of one equivalent of (pin^F)²⁻ ligand per V center and the large reorganizational energy related to dimerization. The voltammogram of 3a under N2 reveals a quasi-reversible V^{IV/V} redox couple at -865 mV. While the presence of this V^{IV/V} redox couple indicates that a dimeric, reduced V(IV) bis- μ -O complex, $[V(O)(\mu$ -O)(pin^F)]₂⁴⁻, may be formed

transiently, the broadened peak shape suggests a large conformational change in the complex upon reduction in aprotic media.

While **3a** displays a single quasi-reversible V^{IV/V} couple at –865 mV, reduced V(IV) dimer **4a** displays a quasi-reversible couple V^{IV/V} at 635 mV and an irreversible oxidation at 1125 mV. Experiments truncating the scan windows reveal that the oxidation at 1125 mV is dependent on the V^{IV/V} feature at 635 mV, but the feature at 635 mV is completely independent. Together, these observations suggest that the two V(IV) centers in **4a** are in electronic communication: an initial electrochemical oxidation of a single V center within **4a** alters the redox potential of the other V center. Interaction of the two V centers is further corroborated by the broad IVCT band present in the UV-visible absorption spectrum of **4a** (870 nm) as well as solution-state magnetic susceptibility measurements indicating antiferromagnetic (AFM) coupling present between the unpaired spins of the two V(IV) centers. Interestingly, the redox features observed in the cyclic

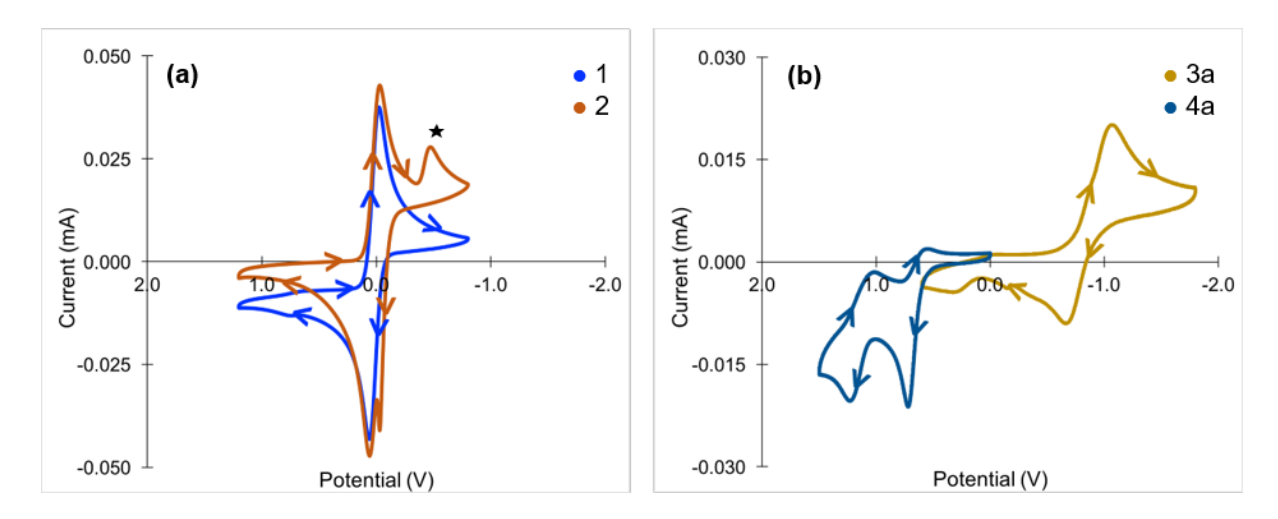
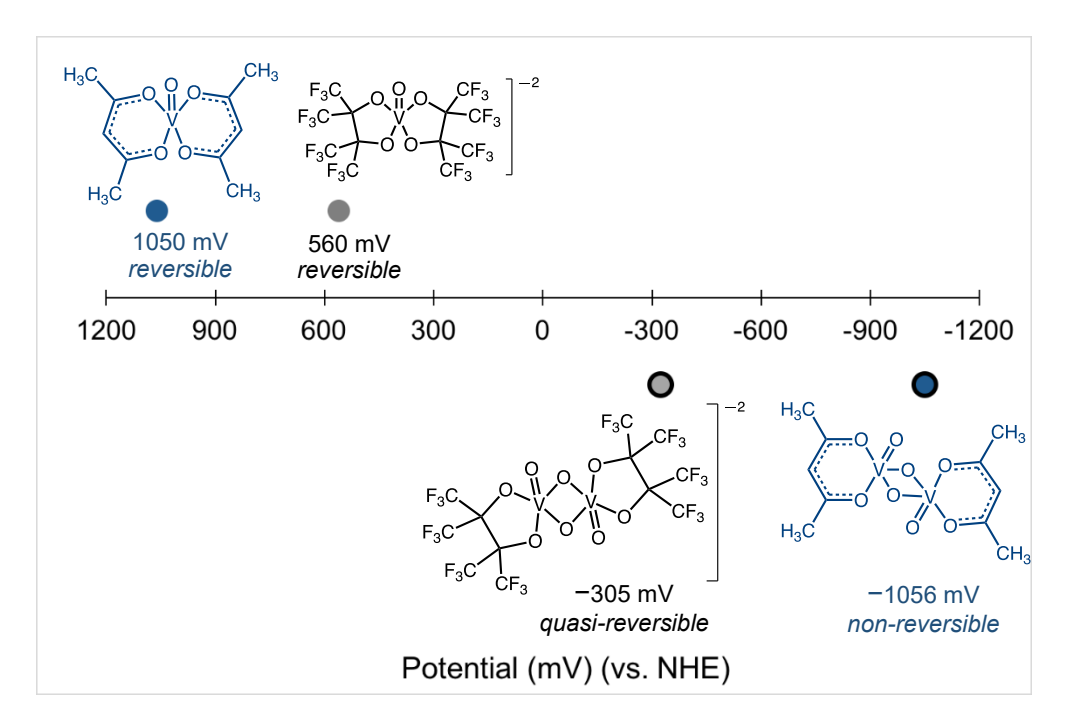


Figure 6. Cyclic voltammograms of 2.5 mM **1**, **2**, **3a**, and **4a** in CH₃CN under N₂ at 100 mV/s with 250 mM Bu₄NPF₆ electrolyte; (a) V-pin^F monomers **1** (blue) and **2** (orange); (b) Vpin^F dimers **3a** (gold) and **4a** (deep blue). The peak centered at −255 mV in (a) corresponds to a small amount of residual Ag in the sample of **2**.

voltammogram of $\mathbf{4a}$ are significantly more positive than the $V^{IV/V}$ couple (near 0 mV) observed for $\mathbf{1}$, indicating that the dimeric compound is more difficult to oxidize and corroborating our observations that $\mathbf{4a}$ is stable for some time in the presence of O_2 .

Table 4. Comparison of V^{IV/V} redox couples of V-pin^F (gray) and V-acac complexes (blue).



To better understand the influence that the $(pin^F)^{2-}$ ligand has on the redox potential of the V centers in the V-pin^F complexes, the redox potentials measured in this work were converted to values versus NHE⁷² and compared to electrochemical data obtained for analogous vanadium acetylacetonate complexes studied by Nawi and coworkers^{73, 74} (Table 4). While 1 displays a reversible V^{IV/V} couple at 560 mV versus NHE, V(O)(acac)₂ is less readily oxidized, with a reversible V^{IV/V} couple at 1050 mV, nearly 500 mV greater than that of 1. Conversely, the quasi-reversible V^{IV/V} peak observed for 3a lies at a moderately negative potential of -305 mV compared to the irreversible V^{IV/V} couple of V₂(O)₂(μ -O)₂(acac)₂ which lies at over -1000 mV. The perfluorinated, dianionic (pin^F)²⁻ ligand distinctly modulates the redox potential of the V-pin^F complexes, making them both easier to oxidize and easier to reduce compared to their V-acac

counterparts. The reason for these differences may lie partly in the ability of the acac ligand to delocalize negative charge within the π -system of the six-membered monoanionic chelate ring, which the sp^3 -pinacolate dianionic chelate cannot do. Therefore the modest additional charge of the mononuclear V^{IV} center is better supported by acac than pin^F. In the dinuclear cases, there are only half as many bidentate ligands per V, such that reduction in the former case is more favorable, although not reversible in either case. Overall, the tolerance of 1 and 3a to air and water combined with their mild potentials form an optimal combination of stability and reactivity, priming the system for redox chemistry.

Within 3a, the readily reducible V(V) centers combined with the Lewis basic (μ -O)₂ bridging moiety, sparked our interest in $[V_2(O)_2(\mu$ -O)_2(pin^F)₂]^{2-} as a motif for formal H₂ storage, in which two protons could be installed on the bridges and two reducing equivalents could be distributed to the V centers. Thus, the reaction of 3a with several H-atom donors was explored (Scheme 3). The highly-activated doubly benzylic alcohol fluorenol was initially selected as a PCET reagent. As shown in Figure 7a, the reaction of 3a with one equivalent of fluorenol in CH₃CN results in an initial color change of the solution from yellow to green. Upon continued stirring, the green solution deepens over the course of a few hours to yield a deep blue solution, consistent with formation of 4a. The initial color change of the solution suggests two possibilities—the solution is simply a mixture of 3a (yellow) and 4a (blue), or, the formation of a green mixed-valent V(IV)/V(V) compound occurs. To probe this mechanistic question, the reaction of 3a with fluorenol was monitored spectroscopically over three hours; the resulting spectra are shown in Figure 7a. Immediately upon reaction, a general increase in the 400 to 1200 nm absorbance range is observed, but as the reaction progresses, the formation of two distinct d-d

Formation of 4a: H-atom transfer to 3a.

(a)
$$F_{3}C CF_{3}$$
 $F_{3}C CF_{3}$ $F_{3}C C$

Scheme 3. Synthesis of **4a** via (a) oxidative alcohol dehydrogenation, demonstrated with fluorenol and (b) PCET, demonstrated with TEMPOH.

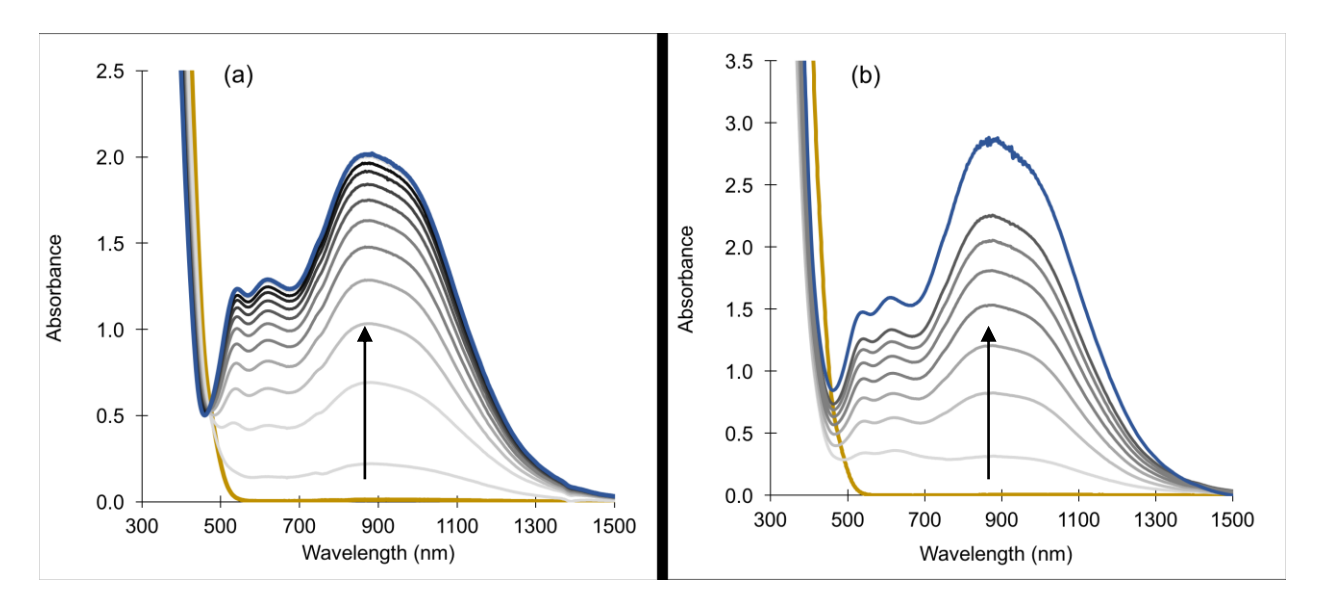


Figure 7. UV-visible absorption spectra showing the formation of **4a** (dark blue traces) from the reaction of **3a** (gold traces) with (a) fluorenol over 3 h and (b) TEMPOH over 12 h.

transitions in the visible region (543, 625 nm) as well an intense, broad peak in the near-IR regime (870 nm) is detected, consistent with the reduction of both d^0 V(V) centers to V(IV) via PCET. Based on the final absorbance value and the extinction coefficients, **4a** is fully formed. While the formation of a V(IV) dimer is evident, no isosbestic points indicating an intermediate species are present in the spectra.

For comparison, the reaction of **3a** with a monoprotic PCET reagent was also investigated using TEMPOH (1-hydroxy-2,2,6,6-tetramethyl-piperidine). Whereas **3a** and fluorenol react in 1:1 ratio to form **4a**, two equivalents of TEMPOH are necessary to fully reduce the V(V) dimer. Similar to the reaction with fluorenol, that of **3a** with two equivalents of TEMPOH in CH₃CN ultimately yields a deep blue solution, although the reaction is much slower, taking approximately twelve hours to go toward completion. As shown in Figure 7b, the UV-vis-NIR spectra tracing the reaction of **3a** with TEMPOH are identical to those with fluorenol and again, no reaction intermediates are observed. Based on the final absorbance value and the extinction coefficients, **4a** is 73% formed after 12 hours.

Additional UV-vis spectroscopy experiments tracing the reaction of **3a** with a single equivalent of TEMPOH produced spectra identical to those in Figure 7 with lower absorbance values, indicating the formation of a smaller amount of fully reduced **4a**, rather than a mixed-valent compound. These results suggest that in the formation of **4a** from **3a**, the initial, formal H-atom abstraction event is the rate-limiting step followed by a faster second H atom abstraction. Spectroscopic studies at low temperatures, at faster scan rates, and/or with different reagents would be necessary to detect any mixed-valent intermediates, and tease apart proton and electron transfer.

Preliminary UV-vis kinetic experiments at a single concentration were performed to determine the thermodynamic parameters associated with PCET for the reaction of 3a with

fluorenol (Figure S6). Experiments performed under pseudo-first order conditions reveal ΔS^{\ddagger} and ΔH^{\ddagger} to be -191 J/mol K and 43.4 kJ/mol, respectively, consistent with a rate-determining associative step.

To investigate the reversibility of PCET, the reaction of **4a** with 2,4,6-tri-*tert*-butylphenoxy radical (2,4,6-TTPR) was examined (Scheme 4a). At room temperature, no reaction between **4a** and the H-atom acceptor occurred. However, heating solutions of **4a** with 2,4,6-TTPR to 40°C resulted in a color change to deep green, suggesting at least the partial re-formation of **3a**. Interestingly, upon removing the solution from heat, the reaction mixture reverted to deep blue and **4a** was recovered.

Unexpectedly, heating 4a above $60^{\circ}C$ (both with or without 2,4,6-TTPR present) resulted in a solution color change from deep blue to purple. Preliminary X-ray diffraction data (Figure S7) of the crystallized purple product indicate the formation of a trimeric V-pin^F species, $\{(Me_4N)[V(O)(\mu_2-O)(pin^F)]\}_3$. Thus, PCET reactions at higher temperature were not pursued in order to preclude trimer formation from 4a.

Although PCET from **4a** to 2,4,6-TTPR to regenerate **3a** was ultimately unsuccessful, the oxidation of **4a** to **3a** was easily accomplished by exposing solutions of **4a** to air (Scheme 4b). Whereas **4a** is stable in air for several days in the solid state, solutions of **4a** convert into **3a** over the course of several hours. The addition of small aliquots of H₂O to solutions of **4a** in air result in the immediate formation of a yellow solution, which suggests that H₂O plays a principal role in the reoxidation process by O₂. Scheme 4c shows the crystal to crystal transformation of **4a** to **3a** after approximately 48 h in air, confirmed via X-ray analysis.

The stoichiometric reactivity of **3a** with H-atom donors and the relative stability of **4a** prompted us to investigate whether this system could oxidize alcohols catalytically. Table 5

(a)
$$F_{3}C CF_{3}$$
 $F_{3}C CF_{3}$ $F_{3}C CF_{3}C CF_{3}$ $F_{3}C CF_{3}C CF_{3}C$

Scheme 4. (a) PCET from **4a** to 2,4,6-TTBPR; (b) exposure of **4a** to air yields quantitative **3a**; (c) transformation of **4a** crystals into **3a** upon exposure to air for 48 h.

summarizes the ability for **3a** to oxidize a variety of alcohols under ambient laboratory conditions with 2 mol% catalyst loading. As with the stoichiometric PCET reactions, the doubly benzylic alcohol, fluorenol, was chosen as an initial substrate. Under these conditions, **3a** was able to oxidize fluorenol with 82% conversion in 48 h. Interestingly, in addition to 9-fluorenone, 2-hydroxy-9-fluorenone was isolated in approximately 15% yield (Figure S8) as a product of fluorenol oxidation. Although unexpected for this system, hydroxylation of the aromatic ring to produce 2-hydroxy-9-fluorenone has been similarly observed in the biotransformation of fluorenol by the fungus *Cunninghamella elegans*. We attempted direct oxidation of fluorenone to 2-hydroxy-9-fluoreneone using **3a** under our standard conditions, however no product formation was witnessed, suggesting incorporation of this hydroxyl moiety occurs only during the oxidation of fluorenol to fluorenone to fluorenone to fluorenone.

Room-temperature catalytic aerobic oxidation of alcohols by 3a.

 Table 5. Catalytic oxidative alcohol dehydrogenation (OAD) reactivity of 3a.

	$\begin{array}{cccccccccccccccccccccccccccccccccccc$				
Subs	trate	Conversion by ¹ H-NMR	Turnover Number	E (V) vs Ag/0.1 N Ag ^{+ b}	pK_a^c
fluor	OH renol	82% 54%ª	27	1.31	13.34
cinnamy	OH l alcohol	40% 35% ^a	18	1.36	14.61
benzyl	OH alcohol	7%	4	> 2.0	14.36
α-methylber	OH nzyl alcohol	3%	1		14.43
cyclohexar	OH nemethanol	0%	N/A		15.17
1,2-benzene	OH OH edimethanol	0%	N/A		13.96
	^a Isolated Yield, ^b see ref ⁷⁵ ^c computational values from SciFinder ⁷⁶				

Additionally, the substrate scope listed in Table 5 encompasses allylic, primary and secondary benzylic alcohols. Cinnamyl, benzyl, and α -methylbenzyl alcohols were oxidized by **3a** to their corresponding aldehydes/ketones as their sole reaction products in 40, 7, and 3% yield, respectively – a range similar to that observed for Limberg's V-thiacalixarene system.^{48, 50}

In each case, upon substrate addition, the initial yellow solution of 3a immediately turned brown/orange; as catalysis progressed, the solution became slightly green. These color changes suggest an initial binding event of the substrate at the oxophilic V center(s), followed by the transient formation of blue 4a during the catalytic process. While the aliphatic substrate cyclohexanemethanol did not react with 3a, benzylic diol 1,2-benzenedimethanol immediately formed an orange/brown solution upon addition of catalyst and no oxidized products were detected by ¹H NMR after 48 h. In this latter case, we hypothesize that the diol coordinates to the oxophilic V center irreversibly such that catalysis cannot occur. When 50 equivalents of 1,2benzenedimethanol are reacted with 3a, 51V-NMR spectra clearly show a change in chemical shift and the relative integration for two NMR signals. New signals appear at -421.21 and -478.91 ppm (Figure S9) in a 1.9:1 ratio (compared with equal intensity -460.67 and -465.86 ppm for **3a**). This result suggests a new chemical environment around the V-centers. The ¹⁹F-NMR spectrum of 3a shows four multiplets between -70.20 and -71.10 ppm, as described above, that change to three distinct singlets at -69.45, -70.72, and -70.84 ppm in a 0.1:1:1.9 ratio (Figure S10), suggesting a new environment about the fluorine atoms, upon reaction with the diol. Neither new compound has yet been isolated, but we tentatively propose the anion $[V(O)(pin^F)\{1,2-(OCH_2)_2C_6H_4\}]^{1-}$ may be present. This result is consistent with our observation that monomerization occurs with an excess of Lewis base, like THF (Scheme 2).

Table S1 summarizes a series of reactions carried out to investigate the role of catalyst loading, desiccant or other additives, temperature, and reaction time, exemplified for benzyl alcohol. In general, an increase in temperature up to 60°C resulted in an increase in the production of benzaldehyde, although reactions were largely carried out at room temperature due to trimerization of 3a at elevated temperatures (*vide supra*). Larger catalyst loadings and the presence of desiccants or other additives resulted in a small increase in the yield of oxidized product. Furthermore, reactions carried out under a balloon of O₂, rather than ambient air, did not show a significant increase in yield.

Although the substrate range of 3a's oxidative capability is limited to allylic and benzylic alcohols, the system's selectivity in not forming carboxylic acid-containing products is notable as the progressive oxidation of alcohols to aldehydes to carboxylic acids is thermodynamically downhill and the isolation of partially oxidized products remains a challenging aspect of VOx surface chemistry. To investigate further the selectivity of our system, 3a was dissolved in neat benzaldehyde (approximately 5 mL) and stirred open to air. Immediately, off-white crystals of benzoic acid began forming throughout the flask and continued stirring produced several grams of the white solid. While 3a is clearly capable of oxidizing benzaldehyde, and qualitatively at a much a faster rate than benzyl alcohol, it does not do so during the catalytic benzyl alcohol oxidations. This result corroborates recent work by Sankar and coworkers which revealed that benzoic alcohol inhibits the oxidation of benzaldehyde due to the interception of intermediate benzoylperoxy radical species by benzyl alcohol.⁷⁸

A proposed catalytic cycle for the oxidation of benzylic alcohols to benzaldehydes by **3a** in air is shown in Figure 8, exemplified by fluorenol. Initially, **3a** reacts with fluorenol via two PCET steps to yield **4a** and an equivalent of ketone. Current data do not allow more detailed description of the

proton and electron transfer sequence, but the known alcohol redox potentials and the calculated pK_a data available, collected in Table 5, suggest that the reaction rate is limited by the potential of

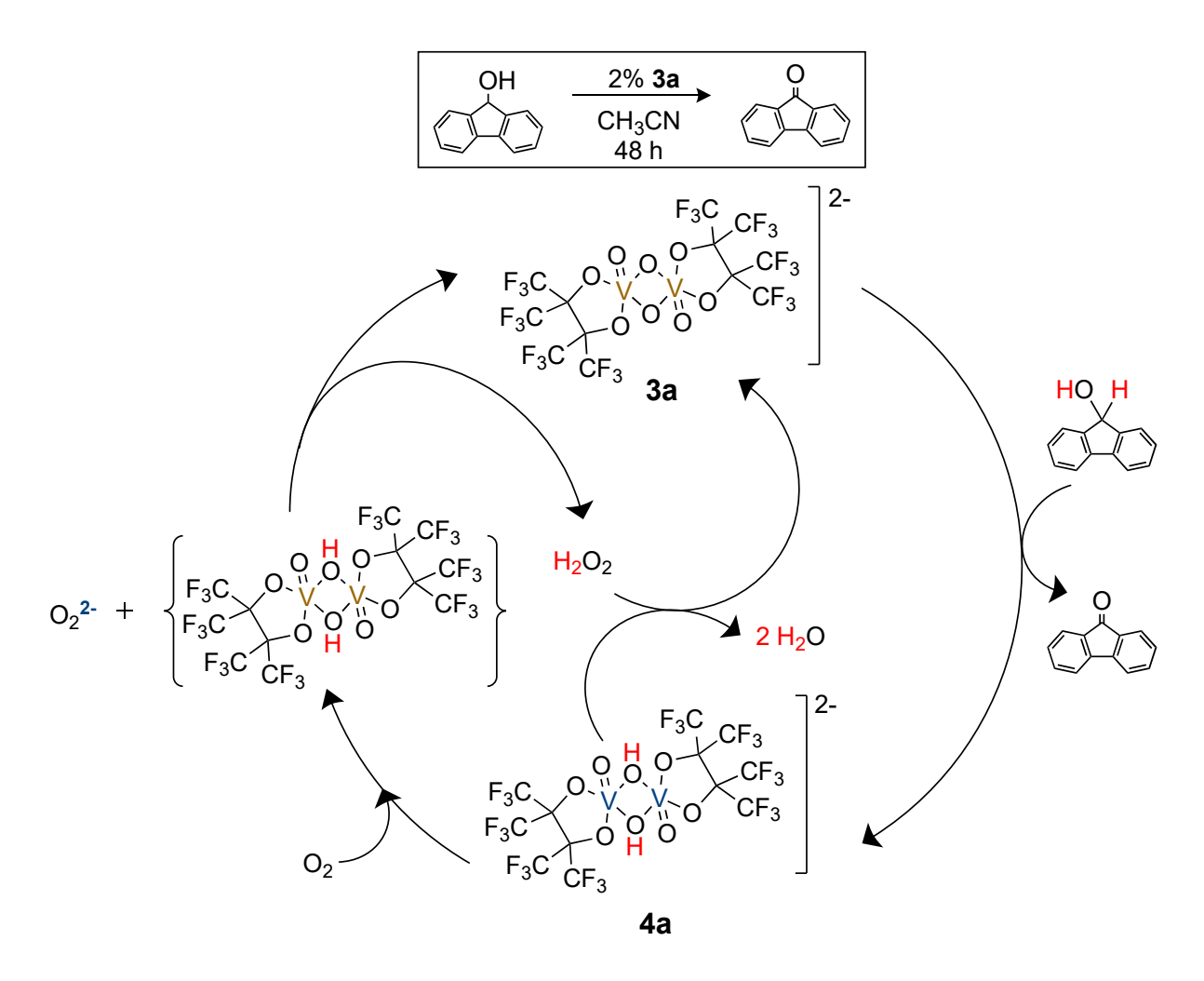


Figure 8. Catalytic aerobic oxidation of fluorenol to fluorenone by 3a via 4a.

the alcohol. The proposed reoxidation of $\mathbf{4a}$ to $\mathbf{3a}$ begins with intermediate formation of an oxidized V(V) (μ -OH)₂ dimer via O₂ reduction, concomitant with the transient formation of (O₂)². The peroxide dianion is protonated by the Brønsted acidic (μ -OH)₂ bridge, forming H₂O₂ and regenerating $\mathbf{3a}$. Finally, the equivalent of H₂O₂ formed *in situ* oxidizes an additional equivalent of $\mathbf{4a}$, regenerating $\mathbf{3a}$ and producing two equivalents of H₂O as the final product of O₂ reduction. Alternatively (and not shown), H₂O₂ could disproportionate into H₂O and O₂, and O₂ continues

the oxidation. Further work is underway to expand on this mechanistic proposal and further define the substrate scope.

Conclusions

Past focus on the synthesis, characterization, and reactivity of first-row transition metal complexes stabilized by highly-fluorinated O-donor ligands has recently expanded to include V=O complexes containing oxidatively-robust, electron-withdrawing perfluoropinacolate (pin^F) ligands. Upon exposure to air, monomeric V(IV) and V(V) complexes 1 and 2 eventually form low yields of 3a, a $(\mu$ -O)₂-bridged V(V) dimer, although the deliberate synthesis of 3a from 1 was also achieved by adjusting the V:pin^F stoichiometry and employing H₂O₂/CH₃CN as an oxidant. The catalytic oxidation of several activated benzylic alcohols to the corresponding aldehyde, and benzaldehyde to benzoic acid, by 3a were observed, proceeding at room-temperature and without the use of stoichiometric additives. Stoichiometric PCET to 3a from either TEMPOH or activated alcohols results in the formation of 4a, a (μ-OH)₂-bridged V(IV) dimer. The structural characterization of $[V(O)_2(\mu-OH)_2(pin^F)_2]^{2-}$ was made possible by utilizing K⁺ encapsulated by 18-crown-6 as counter-cations, which stabilize the system through K... O interactions between the counter ion and terminal oxo moiety and H-bonding between the μ -OH bridge and the crown ether, resulting in 4b. Finally, compared to their non-fluorinated V(O)-acac relatives, 1 and 3a are both easier to oxidize and reduce, demonstrating the effect of the dianionic, perfluorinated pin^F ligand in modulating the metal redox potential. Solution and solid state magnetic susceptibility studies demonstrated antiferromagnetic coupling of the two V(IV) d^1 centers.

Experimental

General procedures. 1 and 3a/3b were prepared in air; synthesis and manipulations of 2 and 4a/4b were performed in an N₂-filled MBraun dry box. For the synthesis of 1 and 3a/3b, deionized H₂O and laboratory-grade MeOH were utilized; crystallization solvents CH₃CN and Et₂O were dried over 3 Å sieves and used without further purification. For the synthesis of 2 and 4, CH₃CN was dried by refluxing over CaH₂ under N₂, distilling, and stored over 3 Å molecular sieves in the dry box. Anhydrous Et₂O was dried in an alumina-based solvent purification system (SPS) under Ar, piped directly into the N₂-filled dry box, and stored over 3 Å molecular sieves. H₂pin^F was purchased from Oakwood Chemicals and stored over 3 Å molecular sieves. Celite was heated to 125°C under vacuum overnight and stored under N₂. Reagents TEMPOH (1-hydroxy-2,2,6,6tetramethyl-piperidine) and TTBPR (2,4,6-tri-tert-butylphenoxy radical) were prepared according to established literature procedures. 79-81 All other reagents were obtained commercially and used with further purification. Standard UV-vis data were collected with a Shimadzu UV-3600 spectrometer while kinetic data was obtained using UV-visible absorption spectroscopy collected with a Cary 300 spectrometer. Elemental analyses were performed by Atlantic Microlabs, Inc. (Norcross, GA).

Cyclic voltammetry. Cyclic voltammetry studies were performed under N₂ using a concentration of 2.5 mM of each complex and 250 mM of Bu₄NPF₆ as the supporting electrolyte in anhydrous CH₃CN. Supporting electrolyte Bu₄NPF₆ was obtained commercially and recrystallized twice from EtOH. A standard three-electrode cell connected to an external CHI 630C potentiostat powered by a personal computer with CHI software was used. A glassy carbon electrode (0.5 mm diameter) was employed as the working electrode, Ag/AgNO₃ electrode as the reference electrode, and Pt

wire as the counter electrode, respectively. The working electrode was rinsed and polished between experiments using polishing alumina and a fine grit pad. Unless otherwise noted, all voltammograms were recorded at a 100 mV/s scan rate.

NMR spectroscopy and Evans method measurements. ¹H-NMR, ¹⁹F-NMR, and ⁵¹V-NMR spectra were recorded at 117.42 kG (¹H 500 MHz, ¹⁹F 470 MHz, ⁵¹V 131 MHz) at ambient temperature using a Varian Agilent 500 MHz VNMRS spectrometer at Boston University Chemical Instrumentation Center (BU-CIC). ¹³C-NMR were recorded at 140.94 kG (¹³C 151 MHz) using a 4-channel Bruker Avance Neo 600 MHz spectrometer equipped with a heliumcooled QCI-F cryoprobe at Massachusetts Institute of Technology Department of Chemistry Instrumentation Facility (MIT-DCIF). Proton chemical shifts are expressed in parts per million (ppm) relative to the residual protio solvent resonance in the solvents as follows: CD₃CN δ 1.94, $(CD_3)_2CO \delta 2.05$, $(CD_3)_2SO \delta 2.50$. For ¹³C spectra, the CD₃CN signal at δ 118.26 was used as internal reference. For ¹⁹F spectra of **3a** and **3b** in CD₃CN, a coaxial tertiary internal NMR standard containing 0.100 M trifluorotoluene in CD₃CN (δ -63.10) was used, following the method described by Rosenau et al.⁸²For all other ¹⁹F-NMR spectra, neat CFCl₃ (δ 0.00) was used as an external reference. For ⁵¹V spectra, a sealed capillary internal standard containing neat VOCl₃ (δ 0.00) was used as an internal reference. Data are reported as follows: chemical shifts, multiplicity (br s = broad singlet, s = singlet, d = doublet, t = triplet, q = quartet, m = multiplet, overlap = overlapping signals) expressing coupling constant(s) in hertz (Hz), and integration. NMR samples of **3a** and **3b** were acquired at 50.0 mM concentration.

Solution-state magnetic susceptibilities were determined via Evans method in CD₃CN, with (Me₃Si)₂O as an internal reference. Values are reported taking into account appropriate diamagnetic corrections.^{83,84}

SQUID magnetometry. Magnetic susceptibility data for 4b were collected with a Quantum Design MPMS3 Evercool SQUID magnetometer in the temperature range 2-300 K at applied fields of 0.1 T and 0.5 T. Samples were ground into fine microcrystalline powders, packed loosely into a polyethylene bag, heat sealed, and inserted into straws (Quantum Design #8000-001) under an N₂ environment prior to analysis. The absence of ferromagnetic impurities was confirmed for by observing a linear relationship between magnetization and applied field (0.1-7.0 T) at 100 K. For all measurements, diamagnetic corrections were applied by using Pascal's constants and by subtracting the diamagnetic susceptibility from the sample holder.⁸⁵

Catalytic alcohol oxidation reactions. The ability of 3a to catalyze the oxidation of alcohols, including fluorenol, cinnamyl alcohol, benzyl alcohol, α-methylbenzyl alcohol, cyclohexanemethanol, and 1,2-benzenedimethanol, at room-temperature under ambient conditions was investigated as follows: Initially, 50 equivalents of alcohol were dissolved in 4.0 mL of CD₃CN in a scintillation vial; an aliquot of solution was used to obtain an ¹H NMR spectrum in order to confirm the purity of the starting alcohols, due to the susceptibility of several of the substrates to autoxidize in air. Subsequently, the aliquot was returned to solution and a single equivalent of 3a (5.0 mg, 5.1 μmol) in 1.0 mL of CD₃CN was added to the solution. The solutions were stirred open to air for 48 h and, due to the evaporation of CD₃CN over time, portions of CD₃CN were added at regular intervals to maintain total solution volume of 5 mL. After 48 h, an

¹H NMR was obtained in order to determine percent conversion. For fluorenol and cinnamyl alcohol, isolated yields were also calculated after chromatographic purification of the reaction mixture as specified in the supplementary information.

1 (Me₄N)₂[V(O)(pin^F)₂]. V(O)SO₄*xH₂O (0.150 g, 0.920 mmol) was dissolved in 6 mL of a 5:1 H₂O:MeOH solution, yielding a blue solution. H₂pin^F (0.615 g, 1.840 mmol) was added directly to the solution and the reaction mixture stirred for 20 min. Me₄NOH•5H₂O (0.667 g, 3.681 mmol) was dissolved in 8 mL of H₂O and half of the solution was added dropwise to the reaction mixture, yielding a bright blue precipitate. After stirring for 1 h, the remainder of the base solution was added dropwise and the reaction mixture stirred for 6 h, forming a pale blue precipitate. The pale blue solid was collected on a frit and rinsed thoroughly with H₂O. Bright blue needles (0.343 g, 42% yield) were grown by layering CH₃CN/Et₂O at 5°C. UV-vis (CH₃CN) (λ_{max} , nm (ϵ , M⁻¹ cm⁻¹)): 361 (42), 564 (23), 624 (25). Anal. calcd. for C₂₀H₂₄F₂₄N₂O₅V: C, 27.32; H, 2.75; N, 3.19. Found: C, 27.41; H, 2.83; N, 3.45. μ_{eff} (CD₃CN) = 1.42(5) μ_{B} . IR: $\nu_{V=O}$ = 967 cm⁻¹.

2 (Me₄N)[V(O)(pin^F)₂]. In a N₂-filled glove box, **1** (0.300 g, 0.341 mmol) was dissolved in 8 mL of CH₃CN, yielding a blue solution. AgPF₆ (0.104 g, 0.409 mmol) was dissolved in 2 mL of CH₃CN and added dropwise to the stirring solution of complex. The reaction mixture was stirred in the dark for 6 h, affording a cloudy orange solution. The solution was concentrated under vacuum to 3 mL and filtered through Celite, yielding a translucent, bright yellow/orange solution. Bright orange blocks (0.196 g, 71% yield) were grown by layering CH₃CN/Et₂O at -28°C. UV-vis (CH₃CN) (λ_{max}, nm (ε, M⁻¹ cm⁻¹)): 330 (6137), 438 (3985). Anal. calcd. for C₁₆H₁₂F₂₄NO₅V:

C, 23.87; H, 1.50; N, 1.74. Found: C, 23.89; H, 1.31; N, 1.75. ¹H NMR (CD₃CN, 500 MHz), 3.05 ppm (s); ¹⁹F NMR (CD₃CN, 500 MHz), -70.3 ppm (m), -71.1 ppm (m). IR: $v_{V=O} = 1011.13 \text{ cm}^{-1}$.

3a $(Me4N)_2[V_2(O)_2(\mu-O)_2(pin^F)_2]$. $V(O)SO_4 \circ xH_2O$ (0.200 g, 1.227 mmol) was dissolved in 6 mL of a 5:1 H₂O:MeOH solution, yielding a blue solution. H₂pin^F (0.409 g, 1.227 mmol) was added directly to the solution and the reaction mixture stirred for 20 min. Me₄NOH•5H₂O (0.444 g, 2.454 mmol) was dissolved in 5 mL of H₂O and added. The solution was stirred for several minutes and added dropwise to the reaction mixture, forming an indigo solution and a sticky deep blue precipitate. 4 mL of CH₃CN and an excess of H₂O₂ (30% aq. solution, 10 drops) was added to the reaction mixture over 20 min and the solution became cloudy green. Upon concentrating the solution at 100°C, a bright yellow solid precipitated, leaving behind a pale blue solution. The yellow solid was collected on a frit and rinsed thoroughly with H₂O. Bright yellow crystalline needles (0.672 g, 56% yield) were grown by layering CH₃CN/Et₂O at 5°C. UV-vis (CH₃CN) (λ_{max} , nm (ϵ , M^{-1} cm $^{-1}$)): 252 (7062), 355 (2402). Anal. calcd. for $C_{20}H_{24}F_{24}N_2O_8V_2$: C, 24.56; H, 2.47; N, 2.86. Found: C, 24.86; H, 2.40; N, 2.88. ¹H-NMR (500 MHz, CD₃CN): δ 3.09 (t, ² J_{HN} = 0.5 Hz, 24H). ¹³C-NMR (151 MHz, CD₃CN): δ 124.09, 124.03, 123.91, 123.84, 95.91, 95.88, 56.14 (t, $^{1}J_{\text{CN}} = 4.0 \text{ Hz}$). $^{19}\text{F-NMR}$ (470 MHz, CD₃CN): δ -70.32 (m), -70.53 (m), -70.86 (m), -70.98 (m). ⁵¹V-NMR (131 MHz, CD₃CN): δ -460.67, -465.86.

3b {**K**(18C6)}2[**V**₂(**O**)₂(**pin**^F)2]. V(O)SO₄•xH₂O (0.200 g, 1.227 mmol) was dissolved in 6 mL of a 5:1 H₂O:MeOH solution, yielding a blue solution. H₂pin^F (0.409 g, 1.227 mmol) was added directly to the solution and the reaction mixture stirred for 20 min. KOH (0.138 g, 2.454 mmol) was dissolved in 5 mL of H₂O and 18-crown-6 (0.324 g, 1.227 mmol) added. The solution

was stirred for several minutes and added dropwise to the reaction mixture, forming an indigo solution and a sticky deep blue precipitate. 4 mL of CH₃CN and an excess of H₂O₂ (30% aq. solution, 8 drops) was added to the reaction mixture over 20 min and the solution became cloudy green. Upon concentrating the solution at 100°C, a bright yellow solid precipitated, leaving behind a pale blue solution. The yellow solid was collected on a frit and rinsed thoroughly with H₂O. Bright yellow crystalline blocks (0.758 g, 43% yield) were grown by layering CH₃CN/Et₂O at 5°C. Anal. calcd. for C₃₆H₄₈F₂₄K₂O₂₀V₂: C, 30.09; H, 3.37; N, 0.00. Found: C, 30.08; H, 3.39; N, 0.00. ¹H-NMR (500 MHz, CD₃CN): δ 3.57 (s, 48H). ¹³C-NMR (151 MHz, CD₃CN): δ 124.15, 123.98, 123.87, 95.87, 95.73, 70.86. ¹⁹F-NMR (470 MHz, CD₃CN): δ -70.29 (m), -70.48 (m), -70.80 (m), -71.01 (m). ⁵¹V-NMR (131 MHz, CD₃CN): δ -457.76, -463.71.

4a (Me₄N)₂[V₂(O)₂(μ-OH)₂(pin^F)₂]. In a N₂-filled glove box, **3a** (0.300 g, 0.307 mmol) was dissolved in 6 mL of CH₃CN, yielding a bright yellow solution. Fluorenol (0.031 g, 0.307 mmol) was dissolved in 3 mL of CH₃CN, added to the stirring solution of complex, and the solution stirred for 3.5 h. The resultant deep indigo-blue solution was dried under vacuum and the resulting sticky blue solid was triturated thrice with Et₂O, stirred in CH₂Cl₂ to extract the fluorenone byproduct, and collected on a frit. The pale blue solid was redissolved in minimal CH₃CN and filtered through Celite, yielding a deep blue solution. Pale blue needles (0.168 g, 56% yield) were grown by layering CH₃CN/Et₂O at room temperature. UV-vis (CH₃CN) (λ_{max} , nm (ε , M⁻¹ cm⁻¹)): 543 (283), 625 (315), 870 (542). Anal. calcd. for C₂₂H₂₉F₂₄N₃O₈V₂: C, 25.87; H, 2.86; N, 4.11. Found: C, 26.12; H, 2.70; N, 3.72. IR: $\upsilon_{V=O} = 963$ cm⁻¹.

4b {K(18C6)}2[V2(O)2(μ-OH)2(pin^F)2]. In a N2-filled glove box, **3b** (0.240 g, 0.167 mmol) was dissolved in 5 mL of CH₃CN, yielding a bright yellow solution. Fluorenol (0.030 g, 0.167 mmol) was dissolved in 2 mL of CH₃CN, added to the stirring solution of complex, and the solution stirred for 3.5 h. The resultant deep indigo-blue solution was dried under vacuum and the resulting sticky blue solid was triturated thrice with Et₂O, stirred in CH₂Cl₂ to extract the fluorenone byproduct, and collected on a frit. The pale blue solid was redissolved in minimal CH₃CN and filtered through Celite, yielding a deep blue solution. Pale blue needles (0.087 g, 36% yield) were grown by layering CH₃CN/Et₂O at room temperature. UV-vis (CH₃CN) (λ_{max} , nm (ε , M⁻¹ cm⁻¹)): 548 (290), 635 (338), 875 (560). Anal. calcd. for C₃₆H₅₀F₂₄K₂O₂₀V₂: C, 30.05; H, 3.50; N, 0.00. Found: C, 30.27; H, 3.57; N, 0.00. μ_{eff} (CD₃CN) = 1.14(1) μ_B.

Acknowledgements

We thank Prof. Mike Graf (Department of Physics, Boston College) for access to and assistance with the SQUID magnetometer at Boston College. We thank Dr. Jeffrey Bacon (Boston University) for obtaining X-ray crystallographic data for 2-hydroxy-9-fluorenone and Dr. Norman Lee (Boston University) for obtaining high-resolution mass spectrometry data for the 2-hydroxy-9-fluorenone product isolated from fluorenol oxidation. We thank Dr. Paul Ralifo (Boston University) and Dr. Walt Massefski (Massachusetts Institute of Technology, Department of Chemistry Instrumentation Facility) for assistance with ⁵¹V-NMR and ¹⁹F-decoupled ¹³C-NMR acquisition, respectively. We are grateful to the National Science Foundation (NSF) for support of this work (CHE 01800313 to LHD, CHE 0619339 to BU for the NMR spectrometer, DMR 1337567 to BC for the SQUID magnetometer, and CHE 01560152 REU, SLC).

Supporting Information

The electronic supporting information includes crystallographic data collection and refinement parameters, ¹⁹F-NMR of **3a** in CD₃CN, (CD₃)₂CO, and (CD₃)₂SO, ¹⁹F NMR data for **2**, ¹H-, ¹³C-, ¹⁹F-, ⁵¹V-NMR of **3a** and **3b** in CD₃CN, SQUID magnetometry of **4b**, electrochemical scan rate dependence studies of **1**, and the Eyring plot for PCET from fluorenol to **3a** to form **4a**. The CCDC deposition numbers for **1**, **2**, **3a**, **3b**, **and 4b** are 1998578-1998582 respectively, and that for 2-hydroxy-9-fluorenone is 2033316.

References

- 1. Tojo, G.; Fernandez, M. I., Oxidation of Alcohols to Aldehydes and Ketones: A Guide to Current Common Practice. Springer US: 2006.
- 2. Dess, D. B.; Martin, J. C., Readily Accessible 12-I-5 Oxidant for the Conversion of Primary and Secondary Alcohols to Aldehydes and Ketones. *J. Org. Chem.* **1983**, *48* (22), 4155-4156.
- 3. Frigerio, M.; Santagostino, M., A Mild Oxidizing Reagent for Alcohols and 1,2-Diols: *o*-Iodoxybenzoic Acid (IBX) in DMSO. *Tetrahedron Lett.* **1994,** *35* (43), 8019-8022.
- 4. Plumb, J. B.; Harper, D. J., 2-Iodoxybenzoic acid. *Chem. Eng. News* **1990**, *68* (29), 2-3,45.
- 5. Mancuso, A. J.; Brownfain, D. S.; Swern, D., Structure of the Dimethyl Sulfoxide-Oxalyl Chloride Reaction Product. Oxidation of Heteroaromatic and Diverse Alcohols to Carbonyl Compounds. *J. Org. Chem.* **1979**, *44* (23), 4148-4150.
- 6. Mancuso, A. J.; Huang, S.-L.; Swern, D., Oxidation of Long-Chain and Related Alcohols to Carbonyls by Dimethyl Sulfoxide "Activated" by Oxalyl Chloride. *J. Org. Chem.* **1978**, *43* (12), 2480-2482.
- 7. Omura, K.; Swern, D., Oxidation of Alcohols by "Activated" Dimethyl Sulfoxide. A Preparative, Steric and Mechanistic Study. *Tetrahedron* **1978**, *34* (11), 1651-1660.
- 8. Pfitzner, K. E.; Moffatt, J. G., A New and Selective Oxidation of Alcohols. *J. Am. Chem. Soc.* **1963**, *85* (19), 3027-3028.
- 9. Corey, E. J.; Kim, C. U., New and Highly Effective Method for the Oxidation of Primary and Secondary Alcohols to Carbonyl Compounds. *J. Am. Chem. Soc.* **1972**, *94* (21), 7586-7587.
- 10. Corey, E. J.; Kim, C. U., A Method for the Oxidation of *sec,tert*-1,2-Diols to α-Hydroxy Ketones Without Carbon-Carbon Cleavage. *Tetrahedron Lett.* **1974**, *15* (3), 287-290.
- 11. Parikh, J. R.; Doering, W. v. E., Sulfur Trioxide in the Oxidation of Alcohols by Dimethyl Sulfoxide. *J. Am. Chem. Soc.* **1967**, *89* (21), 5505-5507.
- 12. Collins, J. C.; Hess, W. W.; Frank, F. J., Dipyridine-Chromium(VI) Oxide Oxidation of Alcohols in Dichloromethane. *Tetrahedron Lett.* **1968,** *9* (30), 3363-3366.
- 13. Corey, E. J.; Suggs, J. W., Pyridinium Chlorochromate. An Efficient Reagent for Oxidation of Primary and Secondary Alcohols to Carbonyl Compounds. *Tetrahedron Lett.* **1975**, *16* (31), 2647-2650.
- 14. Agarwal, S.; Tiwari, H. P.; Sharma, J. P., Pyridinium Chlorochromate: An Improved Method for its Synthesis and Use of Anhydrous Acetic Acid as Catalyst for Oxidation Reactions. *Tetrahedron* **1990**, *46* (12), 4417-4420.
- 15. Cornforth, R. H.; Cornforth, J. W.; Popják, G., Preparation of *R* and *S*-mevalonolactones. *Tetrahedron* **1962**, *18* (12), 1351-1354.
- 16. Bowden, K.; Heilbron, I. M.; Jones, E. R. H.; Weedon, B. C. L., 13. Researches on Acetylenic Compounds. Part I. The Preparation of Acetylenic Ketones by Oxidation of Acetylenic Carbinols and Glycols. *Journal of the Chemical Society* **1946**, 39-45.
- 17. Steinhoff, B. A.; Guzei, I. A.; Stahl, S. S., Mechanistic Characterization of Aerobic Alcohol Oxidation Catalyzed by Pd(OAc)₂/Pyridine Including Identification of the Catalyst Resting State and the Origin of Nonlinear [Catalyst] Dependence. *J. Am. Chem. Soc.* **2004**, *126* (36), 11268-11278.

- 18. Steinhoff, B. A.; Stahl, S. S., Mechanism of Pd(OAc)₂/DMSO-Catalyzed Aerobic Alcohol Oxidation: Mass-Transfer-Limitation Effects and Catalyst Decomposition Pathways. *J. Am. Chem. Soc.* **2006**, *128* (13), 4348-4355.
- 19. Hoover, J. M.; Ryland, B. L.; Stahl, S. S., Mechanism of Copper(I)/TEMPO-Catalyzed Aerobic Alcohol Oxidation. *J. Am. Chem. Soc.* **2013**, *135* (6), 2357-2367.
- 20. Hoover, J. M.; Stahl, S. S., Highly Practical Copper(I)/TEMPO Catalyst System for Chemoselective Aerobic Oxidation of Primary Alcohols. *J. Am. Chem. Soc.* **2011**, *133* (42), 16901-16910.
- 21. Hoover, J. M.; Steves, J. E.; Stahl, S. S., Copper(I)/TEMPO-Catalyzed Aerobic Oxidation of Primary Alcohols to Aldehydes with Ambient Air. *Nat. Protoc.* **2012**, *7* (6), 1161-1166.
- 22. Kodama, S.; Ueta, Y.; Yoshida, J.; Nomoto, A.; Yano, S.; Ueshima, M.; Ogawa, A., Tetranuclear Vanadium Complex, (VO)₄(hpic)₄: A Recyclable Catalyst for Oxidation of Benzyl Alcohols with Molecular Oxygen. *Dalton Trans.* **2009**, (44), 9708-9711.
- 23. Wigington, B. N.; Drummond, M. L.; Cundari, T. R.; Thorn, D. L.; Hanson, S. K.; Scott, S. L., A Biomimetic Pathway for Vanadium-Catalyzed Aerobic Oxidation of Alcohols: Evidence for a Base-Assisted Dehydrogenation Mechanism. *Chem. Eur. J.* **2012**, *18* (47), 14981-14988.
- 24. Hoppe, E.; Limberg, C., Oxovanadium(V) Tetrathiacalix[4]arene Complexes and Their Activity as Oxidation Catalysts. *Chem. Eur. J.* **2007**, *13* (24), 7006-7016.
- 25. Argyle, M. D.; Chen, K.; Bell, A. T.; Iglesia, E., Effect of Catalyst Structure on Oxidative Dehydrogenation of Ethane and Propane on Alumina-Supported Vanadia. *J. Catal.* **2002**, *208* (1), 139-149.
- 26. Blasco, T.; Galli, A.; López Nieto, J. M.; Trifiró, F., Oxidative Dehydrogenation of Ethane and *n*-Butane on VO_x/Al₂O₃ Catalysts. *J. Catal.* **1997**, *169* (1), 203-211.
- 27. Blasco, T.; Nieto, J. M. L., Oxidative Dehydrogenation of Short Chain Alkanes on Supported Vanadium Oxide Catalysts. *Appl. Catal.*, *A* **1997**, *157* (1), 117-142.
- 28. Chaar, M. A.; Patel, D.; Kung, H. H., Selective Oxidative Dehydrogenation of Propane Over V-Mg-O catalysts. *J. Catal.* **1988**, *109* (2), 463-467.
- 29. Comite, A.; Sorrentino, A.; Capannelli, G.; Di Serio, M.; Tesser, R.; Santacesaria, E., Oxidative Dehydrogenation of Propane using V₂O₅/TiO₂/SiO₂ Catalysts Prepared by Grafting Titanium and Vanadium Alkoxides on Silica. *J. Mol. Catal. A: Chem.* **2003**, *198* (1), 151-165.
- 30. Corma, A.; Nieto, J. M. L.; Paredes, N., Influence of the Preparation Methods of V-Mg-O Catalysts on Their Catalytic Properties for the Oxidative Dehydrogenation of Propane. *J. Catal.* **1993**, *144* (2), 425-438.
- 31. Eon, J. G.; Olier, R.; Volta, J. C., Oxidative Dehydrogenation of Propane on γ -Al₂O₃ Supported Vanadium Oxides. *J. Catal.* **1994**, *145* (2), 318-326.
- 32. Evans, O. R.; Bell, A. T.; Tilley, T. D., Oxidative Dehydrogenation of Propane Over Vanadia-based Catalysts Supported on High-surface-area Mesoporous MgAl₂O₄. *J. Catal.* **2004**, *226* (2), 292-300.
- 33. Khodakov, A.; Olthof, B.; Bell, A. T.; Iglesia, E., Structure and Catalytic Properties of Supported Vanadium Oxides: Support Effects on Oxidative Dehydrogenation Reactions. *J. Catal.* **1999**, *181* (2), 205-216.
- 34. Khodakov, A.; Yang, J.; Su, S.; Iglesia, E.; Bell, A. T., Structure and Properties of Vanadium Oxide-Zirconia Catalysts for Propane Oxidative Dehydrogenation. *J. Catal.* **1998**, *177* (2), 343-351.

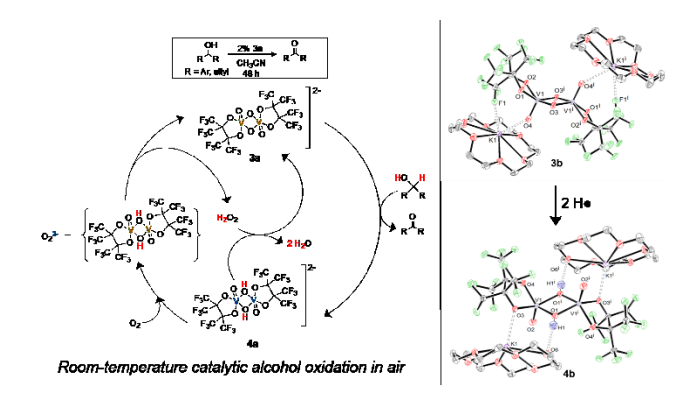
- 35. Kondratenko, E. V.; Baerns, M., Catalytic Oxidative Dehydrogenation of Propane in the Presence of O₂ and N₂O—The Role of Vanadia Distribution and Oxidant Activation. *Appl. Catal.*, A **2001**, 222 (1), 133-143.
- 36. Owens, L.; Kung, H. H., The Effect of Loading of Vanadia on Silica in the Oxidation of Butane. *J. Catal.* **1993**, *144* (1), 202-213.
- 37. Wachs, I. E., Molecular Engineering of Supported Metal Oxide Catalysts: Oxidation Reactions Over Supported Vanadia Catalysts. In *Catalysis*, Spivey, J. J., Ed. The Royal Society of Chemistry: 1997; Vol. 13, pp 37-54.
- 38. Wachs, I. E., Catalysis Science of Supported Vanadium Oxide Catalysts. *Dalton Trans.* **2013**, *42* (33), 11762-11769.
- 39. Zhou, R.; Cao, Y.; Yan, S.; Deng, J.; Liao, Y.; Hong, B., Oxidative Dehydrogenation of Propane over Mesoporous HMS Silica Supported Vanadia. *Catal. Lett.* **2001**, *75* (1), 107-112.
- 40. Kopylovich, M. N.; Ribeiro, A. P. C.; Alegria, E. C. B. A.; Martins, N. M. R.; Martins, L. M. D. R. S.; Pombeiro, A. J. L., In *Adv. Organomet. Chem.*, 2015; pp 91-174.
- 41. Waidmann, C. R.; Zhou, X.; Tsai, E. A.; Kaminsky, W.; Hrovat, D. A.; Borden, W. T.; Mayer, J. M., Slow Hydrogen Atom Transfer Reactions of Oxo- and Hydroxo-Vanadium Compounds: The Importance of Intrinsic Barriers. *J. Am. Chem. Soc.* **2009**, *131* (13), 4729-4743.
- 42. Ohde, C.; Brandt, M.; Limberg, C.; Döbler, J.; Ziemer, B.; Sauer, J., V₂O₅/SiO₂ Surface Inspired, Silsesquioxane-derived Oxovanadium Complexes and Their Properties. *Dalton Trans.* **2008**, (3), 326-331.
- 43. Ohde, C.; Limberg, C.; Stösser, R.; Demeshko, S., Oxovanadium(IV) Silsesquioxane Complexes. *Inorg. Chem.* **2010**, *49* (5), 2479-2485.
- 44. Ohde, C.; Limberg, C., From Surface-Inspired Oxovanadium Silsesquioxane Models to Active Catalysts for the Oxidation of Alcohols with O₂—The Cinnamic Acid/Metavanadate System. *Chem. Eur. J.* **2010**, *16* (23), 6892-6899.
- 45. Hoppe, E.; Limberg, C.; Ziemer, B.; Mügge, C., Vanadium Calixarene Complexes as Molecular Models for Supported Vanadia. *J. Mol. Catal. A: Chem.* **2006,** *251* (1), 34-40.
- 46. Hoppe, E.; Limberg, C.; Ziemer, B., Mono- and Dinuclear Oxovanadium(V)calixarene Complexes and Their Activity as Oxidation Catalysts. *Inorg. Chem.* **2006**, *45* (20), 8308-8317.
- 47. Limberg, C., Calixarene-Based Oxovanadium Complexes as Molecular Models for Catalytically Active Surface Species and Homogeneous Catalysts. *Eur. J. Inorg. Chem.* **2007**, 2007 (21), 3303-3314.
- 48. Werncke, C. G.; Limberg, C.; Knispel, C.; Mebs, S., Surface-Inspired Molecular Vanadium Oxide Catalysts for the Oxidative Dehydrogenation of Alcohols: Evidence for Metal Cooperation and Peroxide Intermediates. *Chem. Eur. J.* **2011**, *17* (43), 12129-12135.
- 49. Werncke, C. G.; Limberg, C.; Knispel, C.; Metzinger, R.; Braun, B., Haloperoxidase Activity of Oxovanadium(V) Thiobisphenolates. *Chem. Eur. J.* **2011**, *17* (10), 2931-2938.
- 50. Werncke, C. G.; Limberg, C.; Metzinger, R., Direct Proof for a Lower Reactivity of Monomeric vs. Dimeric Oxidovanadium Complexes in Alcohol Oxidation. *Z. Anorg. Allg. Chem.* **2013**, *639* (14), 2426-2432.
- 51. Cantalupo, S. A.; Lum, J. S.; Buzzeo, M. C.; Moore, C.; DiPasquale, A. G.; Rheingold, A. L.; Doerrer, L. H., Three-Coordinate Late Transition Metal Fluorinated Alkoxide Complexes. *Dalton Trans.* **2010**, *39* (2), 374-383.
- 52. Cantalupo, S. A.; Ferreira, H. E.; Bataineh, E.; King, A. J.; Petersen, M. V.; Wojtasiewicz, T.; DiPasquale, A. G.; Rheingold, A. L.; Doerrer, L. H., Synthesis with

- Structural and Electronic Characterization of Homoleptic Fe(II)- and Fe(III)-Fluorinated Phenolate Complexes. *Inorg. Chem.* **2011,** *50* (14), 6584-6596.
- 53. Cantalupo, S. A.; Fiedler, S. R.; Shores, M. P.; Rheingold, A. L.; Doerrer, L. H., High-Spin Square-Planar Co(II) and Fe(II) Complexes and Reasons for Their Electronic Structure. *Angew. Chem. Int. Ed.* **2012**, *51* (4), 1000-1005, S1000/1-S1000/18.
- 54. Hannigan, S. F.; Lum, J. S.; Bacon, J. W.; Moore, C.; Golen, J. A.; Rheingold, A. L.; Doerrer, L. H., Room Temperature Stable Organocuprate Copper(III) Complex. *Organometallics* **2013**, *32* (12), 3429-3436.
- 55. Lum, J. S.; Chen, P. E.; Rheingold, A. L.; Doerrer, L. H., Zinc(II) Complexes with Fluorinated Monodentate Aryloxide and Alkoxide Ligands. *Polyhedron* **2013**, *58*, 218-228.
- 56. Lum, J. S.; Tahsini, L.; Golen, J. A.; Moore, C.; Rheingold, A. L.; Doerrer, L. H., K...F/O Interactions Bridge Copper(I) Fluorinated Alkoxide Complexes and Facilitate Dioxygen Activation. *Chem. Eur. J.* **2013**, *19* (20), 6374-6384.
- 57. Tahsini, L.; Specht, S. E.; Lum, J. S.; Nelson, J. J. M.; Long, A. F.; Golen, J. A.; Rheingold, A. L.; Doerrer, L. H., Structural and Electronic Properties of Old and New A₂[M(pin^F)₂] Complexes. *Inorg. Chem.* **2013**, *52* (24), 14050-14063.
- 58. Petersen, M. V.; Iqbal, A. H.; Zakharov, L. N.; Rheingold, A. L.; Doerrer, L. H., Fluorinated Phenolates in Monomeric and Dimeric Co(II) Compounds. *Polyhedron* **2013**, *52*, 276-283.
- 59. Hannigan, S. F.; Arnoff, A. I.; Neville, S. E.; Lum, J. S.; Golen, J. A.; Rheingold, A. L.; Orth, N.; Ivanovic-Burmazovic, I.; Liebhaeuser, P.; Roesener, T.; Stanek, J.; Hoffmann, A.; Herres-Pawlis, S.; Doerrer, L. H., On the Way to a Trisanionic {Cu₃O₂} Core for Oxidase Catalysis: Evidence of an Asymmetric Trinuclear Precursor Stabilized by Perfluoropinacolate Ligands. *Chem. Eur. J.* **2017**, *23* (34), 8320.
- 60. Steele, J. L.; Tahsini, L.; Sun, C.; Elinburg, J. K.; Kotyk, C. M.; McNeely, J.; Stoian, S. A.; Dragulescu-Andrasi, A.; Ozarowski, A.; Ozerov, M.; Krzystek, J.; Telser, J.; Bacon, J. W.; Golen, J. A.; Rheingold, A. L.; Doerrer, L. H., Square-Planar Co(III) in {O₄} Coordination: Large ZFS and Reactivity with ROS. *Chem. Commun.* **2018**, *54* (85), 12045-12048.
- 61. Brazeau, S. E. N.; Norwine, E. E.; Hannigan, S. F.; Orth, N.; Ivanovic-Burmazovic, I.; Rukser, D.; Biebl, F.; Grimm-Lebsanft, B.; Praedel, G.; Teubner, M.; Rubhausen, M.; Liebhauser, P.; Rosener, T.; Stanek, J.; Hoffmann, A.; Herres-Pawlis, S.; Doerrer, L. H., Dual Oxidase/Oxygenase Reactivity and Resonance Raman Spectra of {Cu₃O₂} Moiety with Perfluoro-*t*-butoxide Ligands. *Dalton Trans.* **2019**, *48* (20), 6899-6909.
- 62. Brazeau, S. E. N.; Doerrer, L. H., Cu(I)-O₂ Oxidation Reactions in a Fluorinated All-Odonor Ligand Environment. *Dalton Trans.* **2019**, *48* (15), 4759-4768.
- 63. Willis, C. J., Fluorinated Alkoxides of Chromium(V) and Vanadium(IV). *Chem. Commun.* **1972**, (16), 944-5.
- 64. Payne, G. B., A Simplified Procedure for Epoxidation by Benzonitrile-Hydrogen Peroxide. Selective Oxidation of 2-Allylcyclohexanone. *Tetrahedron* **1962**, *18* (6), 763-765.
- 65. Payne, G. B.; Deming, P. H.; Williams, P. H., Reactions of Hydrogen Peroxide. VII. Alkali-Catalyzed Epoxidation and Oxidation Using a Nitrile as Co-reactant. *J. Org. Chem.* **1961**, *26* (3), 659-663.
- 66. Marzilli, L. G.; Hanson, B. E.; Kistenmacher, T. J.; Epps, L. A.; Stewart, R. C., Isomerism about a Dioxo Bridge. Spectroscopic and Chemical Studies on Oxoosmium(VI) Esters. *Inorg. Chem.* **1976**, *15* (7), 1661-1665.

- 67. Addison, A. W.; Rao, T. N.; Reedijk, J.; van Rijn, J.; Verschoor, G. C., Synthesis, Structure, and Spectroscopic Properties of Copper(II) Compounds Containing Nitrogen—Sulphur Donor Ligands; The Crystal and Molecular Structure of Aqua[1,7-bis(N-methylbenzimidazol-2'-yl)-2,6-dithiaheptane]copper(II) Perchlorate. *Dalton Trans.* **1984**, (7), 1349-1356.
- 68. Casey, C. P., The Structure of Intermediates Formed in the Reaction of Osmium Tetroxide with 1,1-Diphenylethylene. *Chem. Commun.* **1983**, (3), 126-127.
- 69. Schröder, M.; Constable, E. C., Direct Spectroscopic Evidence for the Formation of an Asymmetric Intermediate in the Oxidation of Alkenes by Osmium Tetraoxide. *Chem. Commun.* **1982**, (13), 734-736.
- 70. Ballhausen, C. J.; Gray, H. B., Electronic structure of the vanadyl ion. *Inorg. Chem.* **1962,** *I*, 111-22.
- 71. Nitsche, S.; Schmitz, S.; Stirnat, K.; Sandleben, A.; Klein, A., Controlling Nuclearity and Stereochemistry in Vanadyl(V) and Mixed Valent VIV/VV Complexes of Oxido-Pincer Pyridine-2,6-dimethanol Ligands. Z. Anorg. Allg. Chem. **2018**, 644 (24), 1805-1815.
- 72. Pavlishchuk, V. V.; Addison, A. W., Conversion Constants for Redox Potentials Measured Versus Different Reference Electrodes in Acetonitrile Solutions at 25°C. *Inorg. Chim. Acta* **2000**, *298* (1), 97-102.
- 73. Nawi, M. A.; Riechel, T. L., Electrochemical Studies of Vanadium(V) Acetylacetonate Complexes in Dimethyl Sulfoxide. *Inorg. Chem.* **1982**, *21* (6), 2268-2271.
- 74. Nawi, M. A.; Riechel, T. L., Electrochemical Studies of Vanadium(III) and Vanadium(IV) Acetylacetonate Complexes in Dimethylsulfoxide. *Inorg. Chem.* **1981**, *20* (7), 1974-1978.
- 75. Weinberg, N. L.; Weinberg, H. R., Electrochemical oxidation of organic compounds. *Chem. Rev.* **1968**, *68* (4), 449-523.
- 76. *ACD/Labs*, V11.02; Advanced Chemistry Development 2020.
- 77. Pothuluri, J. V.; Freeman, J. P.; Evans, F. E.; Cerniglia, C. E., Biotransformation of Fluorene by the Fungus *Cunninghamella elegans*. *Appl. Environ*. *Microbiol*. **1993**, *59* (6), 1977.
- 78. Sankar, M.; Nowicka, E.; Carter, E.; Murphy, D. M.; Knight, D. W.; Bethell, D.; Hutchings, G. J., The Benzaldehyde Oxidation Paradox Explained by the Interception of Peroxy Radical by Benzyl Alcohol. *Nat. Commun.* **2014**, *5* (1), 3332.
- 79. Mader, E. A.; Davidson, E. R.; Mayer, J. M., Large Ground-State Entropy Changes for Hydrogen Atom Transfer Reactions of Iron Complexes. *J. Am. Chem. Soc.* **2007**, *129* (16), 5153-5166.
- 80. Manner, V. W.; Markle, T. F.; Freudenthal, J. H.; Roth, J. P.; Mayer, J. M., The First Crystal Structure of a Monomeric Phenoxyl Radical: 2,4,6-tri-*tert*-butylphenoxyl Radical. *Chem. Commun.* **2008**, (2), 256-258.
- 81. Ozinskas, A. J.; Bobst, A. M., Formation of N-Hydroxy-amines of Spin Labeled Nucleosides for ¹H NMR Analysis. *Helv. Chim. Acta* **1980**, *63* (6), 1407-1411.
- 82. Rosenau, C. P.; Jelier, B. J.; Gossert, A. D.; Togni, A., Exposing the Origins of Irreproducibility in Fluorine NMR Spectroscopy. *Angew. Chem. Int. Ed.* **2018**, *57* (30), 9528-9533.
- 83. Evans, D. F., The Determination of the Paramagnetic Susceptibility of Substances in Solution by Nuclear Magnetic Resonance. *J. Chem. Soc.* **1959**, 2003-2005.
- 84. Sur, S. K., Measurement of Magnetic Susceptibility and Magnetic Moment of Paramagnetic Molecules in Solution by High-Field Fourier Transform NMR Spectroscopy. *Journal of Magnetic Resonance* **1989**, *82* (1), 169-173.

85. Bain, G. A.; Berry, J. F., Diamagnetic Corrections and Pascal's Constants. *J. Chem. Educ.* **2008**, *85* (4), 532.

For Table of Contents Only



Caption: An air-stable catalyst for the oxidative dehydrogenation of benzylic alcohols under ambient conditions has been developed.